ASTROBIOLOGY
Volume 3, Number 1, 2003

Rubey Colloquium Paper

Spherule Beds 3.47–3.24 Billion Years Old in the Barberton Greenstone Belt, South Africa: A Record of Large Meteorite Impacts and Their Influence on Early Crustal and Biological Evolution

DONALD R. LOWE,[1] GARY R. BYERLY,[2] FRANK T. KYTE,[3] ALEXANDER SHUKOLYUKOV,[4] FRANK ASARO,[5] and ALEXANDRA KRULL[1]

ABSTRACT

Four layers, S1–S4, containing sand-sized spherical particles formed as a result of large meteorite impacts, occur in 3.47–3.24 Ga rocks of the Barberton Greenstone Belt, South Africa. Ir levels in S3 and S4 locally equal or exceed chondritic values but in other sections are at or only slightly above background. Most spherules are inferred to have formed by condensation of impact-produced rock vapor clouds, although some may represent ballistically ejected liquid droplets. Extreme Ir abundances and heterogeneity may reflect element fractionation during spherule formation, hydraulic fractionation during deposition, and/or diagenetic and metasomatic processes. Deposition of S1, S2, and S3 was widely influenced by waves and/or currents interpreted to represent impact-generated tsunamis, and S1 and S2 show multiple graded layers indicating the passage of two or more wave trains. These tsunamis may have promoted mixing within a globally stratified ocean, enriching surface waters in nutrients for biological communities. S2 and S3 mark the transition from the 300-million-year-long Onverwacht stage of predominantly basaltic and komatiitic volcanism to the late orogenic stage of greenstone belt evolution, suggesting that regional and possibly global tectonic reorganization resulted from these large impacts. These beds provide the oldest known direct record of terrestrial impacts and an opportunity to explore their influence on early life, crust, ocean, and atmosphere. The apparent presence of impact clusters at 3.26–3.24 Ga and ~2.65–2.5 Ga suggests either spikes in impact rates during the Archean or that the entire Archean was characterized by terrestrial impact rates above those currently estimated from the lunar cratering record. Key Words: Impacts—Spherule beds—Archean—Barberton Greenstone Belt. Astrobiology 3, xx–xx.

[1]Department of Geological and Environmental Sciences, Stanford University, Stanford, California.
[2]Department of Geology and Geophysics, Louisiana State University, Baton Rouge, Louisiana.
[3]Center for Astrobiology, Institute of Geophysics and Planetary Physics, University of California, Los Angeles, California.
[4]Scripps Institution of Oceanography, University of California, San Diego, La Jolla, California.
[5]Lawrence-Berkeley Laboratory, University of California, Berkeley, California.

INTRODUCTION

IT IS NOW WIDELY ACCEPTED that meteorite impacts played an important role in the early history of the Earth and life. An exceptionally large impact during accretion may have generated debris from which the Moon formed (Stevenson, 1985, 1987). Late-impacting projectiles probably delivered many of the basic ingredients from which life evolved, including water, atmospheric gases, and organic compounds (Chyba and Sagan, 1997; Delsemme, 1997). Early giant impacts may have also inhibited the evolution and survival of early life forms through global sterilization and modification of surface environments (Sleep *et al.*, 1989; Zahnle and Sleep, 1997). As yet, no unambiguous terrestrial record of this earliest, Hadean impact history is known, but tungsten isotopic anomalies in the 3.7–3.8 Ga Isua Greenstone Belt of West Greenland and related rocks in Labrador may be a geochemical record of the terminal stages of Late Heavy Bombardment (Schoenberg *et al.*, 2002). Most of our understanding of the timing and magnitude of these earliest impacts derives from the cratering record on the Moon (Tera *et al.*, 1974; Ryder, 2002).

However, large impact events were not limited to the Hadean: There is an emerging body of evidence that the Archean geologic record, 3.5–2.5 Ga, preserves a signature of continuing bombardment (Lowe and Byerly, 1986; Lowe *et al.*, 1989; Simonson and Hassler, 2002). Although still not without controversy, this record offers the possibility of directly documenting the effects of impacts on the early evolution of life, surface environments, crust, and ocean and atmosphere.

During studies in the 3.5–3.2 Ga Barberton Greenstone Belt (BGB), South Africa, and Eastern Pilbara Block, Western Australia, Lowe and Byerly (1986) identified layers containing sand-sized spherical particles, termed spherules, which they interpreted to represent quenched liquid silicate droplets. They suggested that these droplets formed as a result of large Archean meteorite or comet impacts. de Wit (1986) proposed that the spherules represent ocelli or variolites eroded from basaltic volcanic rocks. French (1987) noted that silicate spherules are locally associated with the Sudbury impact structure, but were extremely rare, and suggested caution in interpreting the more widespread and abundant Archean spherules as having formed through impact processes. Buick (1987) also suggested that the spherules originated through erosion of basaltic volcanic units.

Lowe and Byerly (1987) discussed the comments of French (l987) and Buick (1987) and suggested that the Archean spherules may have originated through the condensation of globe-encircling clouds of shock-melted and vaporized rock formed during large impacts, a process discussed by Stevenson (1985). Subsequently, Lowe *et al.* (1989) identified four spherule beds in the BGB, termed S1 (lowest) through S4 (highest), and demonstrated that S3 and S4 are sites of major iridium enrichment. Kyte *et al.* (1992) analyzed platinum group elements (PGEs) in S4, noting Ir levels as high as 360 ppb. They noted that S4 contained nearly chondritic relative abundances of Ir, Os, and Pt and attributed fractionation of more mobile Pd and Au to hydrothermal alteration.

Byerly and Lowe (1994) analyzed spinels in S3 spherules. These show dendritic and skeletal octahedral forms, have very high Ni and ferric iron contents, and are composed dominantly of Fe, Ni, Cr, and V. They are distinctly different from those in komatiites and other magmatic rocks and were interpreted to be consistent with formation through condensation of rock vapor clouds following large impacts. The range of spinel compositions was inferred to indicate that there were a variety of spherule types, perhaps representing both metal or sulfide and silicate oxide liquids.

A number of recent investigators have questioned the impact interpretation of the BGB spherule beds (Koeberl *et al.*, 1993; Koeberl and Reimold, 1995; French, 1998; Ryder *et al.*, 2000; Reimold *et al.*, 2000). Koeberl *et al.* (1993), Koeberl and Reimold (1995), and Reimold *et al.* (2000) noted that samples of spherule beds collected in the vicinity of gold mines in the northern BGB show non-chondritic ratios among siderophile elements and a correlation between PGE and chalcophile element abundances. They suggested that elevated PGE levels in the spherule beds are the result of postdepositional mineralization and hydrothermal alteration and that the spherule beds formed through unspecified volcanic processes.

Shukolyukov *et al.* (2000) demonstrated the presence of nonterrestrial Cr isotopic ratios in bed S4, and similar results have now been obtained from S2 and S3 (Kyte *et al.*, 2003). These results have confirmed the presence of a significant extraterrestrial component in the BGB spherule beds and support the impact origin proposed initially based largely on geological arguments.

These units provide a terrestrial record of large meteorite impacts on the early Earth and a key window on the possible role of such impacts on the early evolution of terrestrial life, crust, ocean, and atmosphere. The present report provides a systematic description and interpretation of the four well-studied BGB spherule beds, S1–S4, including type localities, distribution and correlation, characteristics, sedimentology, and implications for the tectonic and impact histories of the early Earth.

GEOLOGIC SETTING

The volcanic and sedimentary sequence in the BGB (Fig. 1) reaches at least 12 km in thickness and has been divided into three major stratigraphic groups (Fig. 2): (1) The lowest, the Onverwacht Group, in classic sections in the southern BGB, includes 8–10 km of largely komatiitic and basaltic volcanic rocks, generally thin interstratified cherty sedimentary layers, and one major dacitic volcanic unit at the top of the Hooggenoeg Formation (Figs. 2 and 3). In the central and northern parts of the belt, north of the Granville Grove Fault (Fig. 3), the Onverwacht Group consists of at least 1,000 m of predominantly komatiitic volcanic and intrusive rocks assigned to the Mendon and Weltevreden Formations. Both include thin interbedded cherty layers and are capped by thick units of black and banded chert (Lowe and Byerly, 1999). (2) The overlying Fig Tree Group, from 500 to ~1,500 m thick, consists of terrigenous sedimentary rocks derived by weathering and erosion of uplifted rocks like those in the underlying Onverwacht Group interbedded with felsic volcaniclastic rocks and cherty strata. (3) The youngest rocks in the BGB belong to the Moodies Group, a clastic unit up to 3,000 m thick composed largely of feldspathic to quartzose sandstone and conglomerate.

The BGB is structurally complex. Virtually all rocks dip vertically to subvertically and are tightly folded and faulted. The southern part of the BGB, south of the Granville Grove Fault (Fig. 3), termed the Songimvelo Block (Lowe *et al.*, 1999), includes a more-or-less continuous section of rocks, 8–10 km thick, from the Komati through Mendon Formations of the Onverwacht Group overlain by 250–300 m of Fig Tree strata (Fig. 2). These units have been folded into large, steep to vertically plunging folds including the Onverwacht Anticline and Kromberg Syncline (Fig. 1). The remainder of the belt consists of a series of east- to northeast-trending fault-bounded structural belts that repeat folded rocks of the Mendon or Weltevreden Formations overlain by sedimentary rocks of the Fig Tree and Moodies Groups. Structural repetition of the Onverwacht–Fig Tree contact provides multiple outcrop belts of spherule beds S2 and S3 across the BGB (Fig. 2).

Although small enclaves locally preserve rocks with near-original mineralogy and composition, most rocks in the Onverwacht and Fig Tree Groups have been affected by postdepositional diagenesis and metasomatism. Komatiitic flow rocks have been widely serpentinized. Sedimentary rocks and flow-surface volcanic units show extensive alteration, including Na, Ca, Fe, and Mg loss; silicification and/or carbonation; and potash enrichment (Smith and Erlank, 1982; Paris *et al.*, 1985; Lowe and Byerly, 1986; Duchac and Hanor, 1987; Hanor and Duchac, 1990; Lowe *et al.*, 1999). However, the timing and mechanics of this alteration remain controversial (compare Paris *et al.*, 1985; Lowe and Byerly, 1986; de Wit and Hart, 1993; Lowe, 1999). Overall, most primary silicate minerals have been altered, although zircons, coarse quartz, chrome-rich spinel, rutile, tourmaline, iron oxides, and sulfide minerals are usually well preserved.

The spherule beds are now composed predominantly of quartz and microcrystalline phyllosilicates, mainly sericite and chlorite. Quartz is principally microquartz (<35 μm), with some coarse quartz occurring mainly as drusy cavity-fill. Common secondary accessory minerals include rutile, apatite, barite, dolomite, and siderite. Metamorphism of rocks of the Onverwacht and Fig Tree Groups most likely reached peak temperatures of ~320°C in the central portions of the BGB (Xie *et al.*, 1997) and 520°C along the southern margin (Cloete, 1999). As a result, most primary feldspars are now represented by albite or quartz-sericite mosaics, and most ferromagnesian minerals by chlorite-actinolite.

Shearing is heterogeneously distributed at a large scale, and over wide areas in the BGB original textures and structures down to 10–20 μm in size are well preserved. This is especially true for cherty layers, which tend to be hard brittle units. Strain during folding and shortening has generally been partitioned into surrounding more ductile volcanic rocks. Extreme alteration, penetrative shearing, structural deformation at all scales,

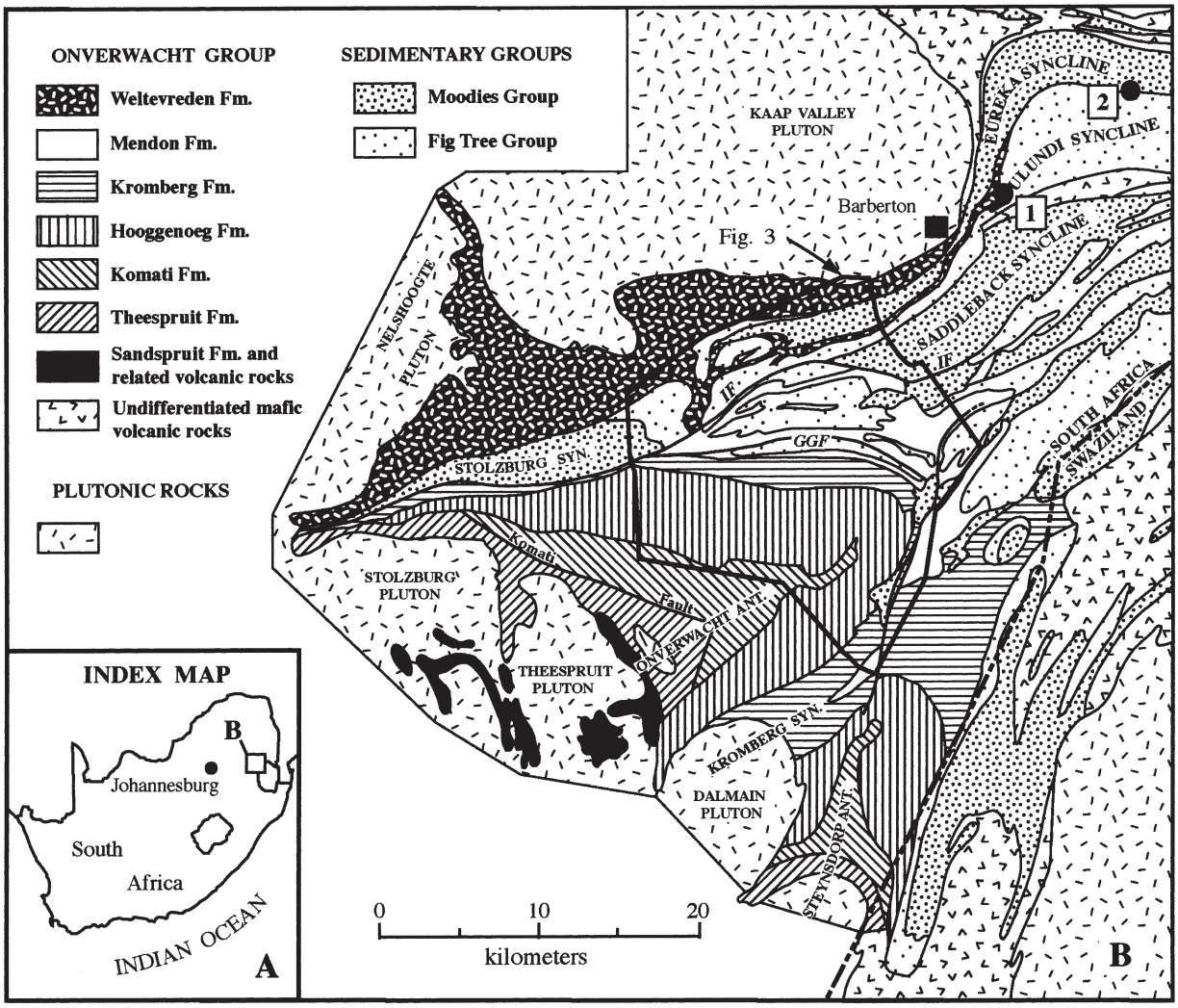

FIG. 1. Generalized geologic map of the western part of the BGB showing the distribution of major stratigraphic units and selected major structural features. Localities (1) and (2) mark the Florence and Devonian Mine (SAF-294) at the south end of the Ulundi Syncline and the Sheba Mine (SAF-381), respectively. Both are sample localities for bed S3. GGF, Granville Grove Fault; IF, Inyoka Fault; Fm., Formation.

and, locally, sulfide mineralization are widely developed along frontal faults in the northernmost BGB, in southeastern and eastern areas along the margins of the belt, and in pre-3,500 Ma parts of the belt.

In the following discussion, individual localities are referred to both by names of local geographic or cultural features (e.g., Sheba Mine) or geologic units (e.g., Jay's chert) and by specific locality numbers, including those of Lowe (SAF localities) and Byerly (SA localities). A list of all localities mentioned in the text, names, numbers, and coordinates is given in Table 1.

T1

SAMPLES AND PROCEDURES

Field identification and study of sample localities discussed in this report are the result of 25 years of field work in the Barberton Belt by D.R.L. and G.R.B. Geochemical analyses were performed over the last 15 years in four laboratories. G.R.B. performed mineral chemical analyses by electron microprobe as described in Byerly and Lowe (1994). Trace element chemistry was performed by F.A. at the University of California at Berkeley and by F.T.K. at UCLA. F.A. measured Ir concentrations by instrumental neutron activa-

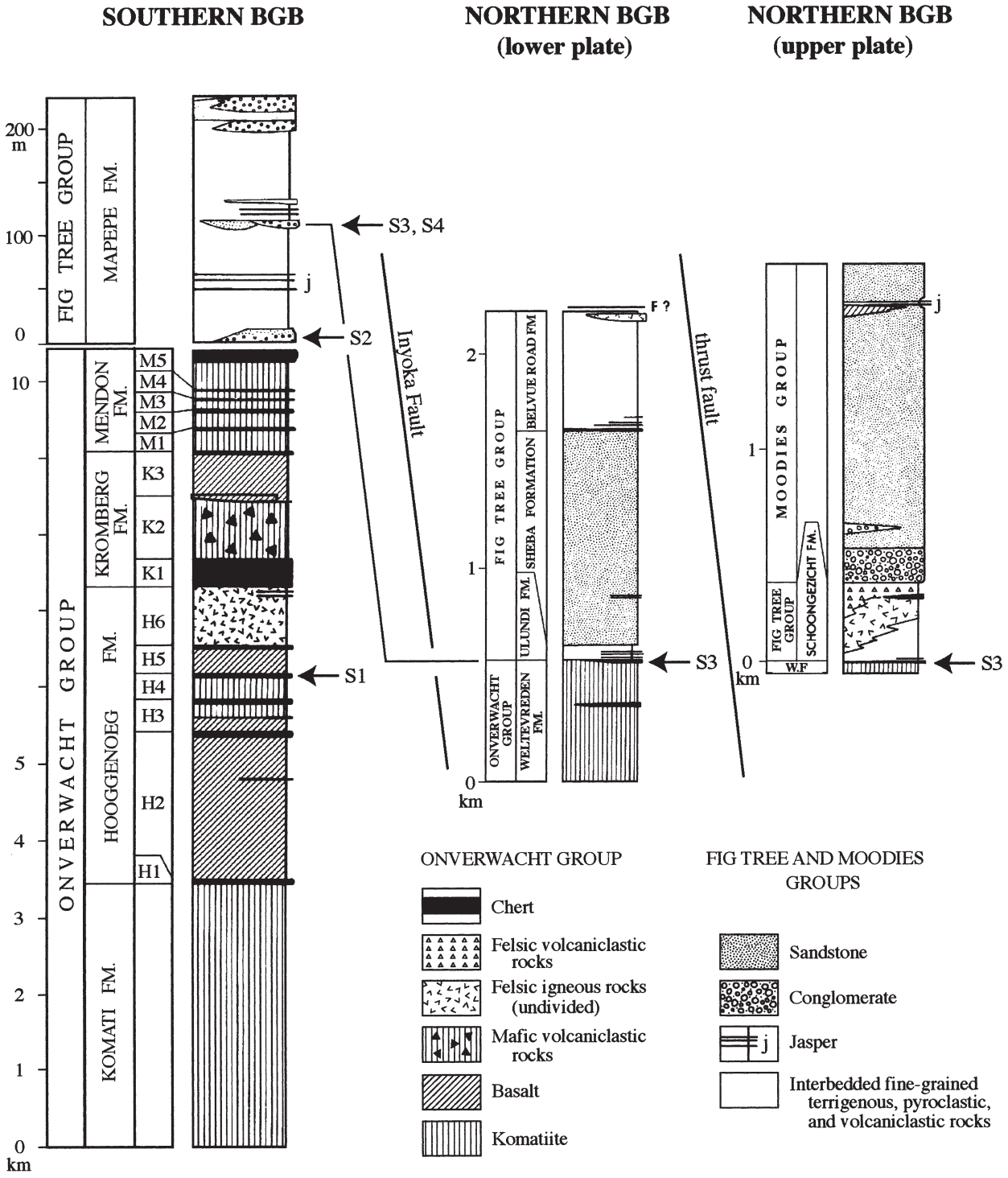

FIG. 2. Stratigraphic sections in the BGB showing the positions of spherule beds S1–S4. As shown here, the southern part of the BGB encompasses the Songimvelo Block of Lowe *et al.* (1999), south of the Granville Grove Fault (Fig. 1), which includes a full section, 10–11 km thick, of the Onverwacht and Fig Tree Groups. The northern BGB includes areas north of the Inyoka Fault (Figs. 1 and 3). Areas between the Granville Grove and Inyoka Faults are made up of the Onverwacht Group, represented only by the 500–1,000–m-thick Mendon Formation, overlain by rocks of the Fig Tree and Moodies Groups. Upper and lower plate rocks in the northern BGB are separated by a regional thrust fault (Lowe *et al.*, 1999). FM., Formation.

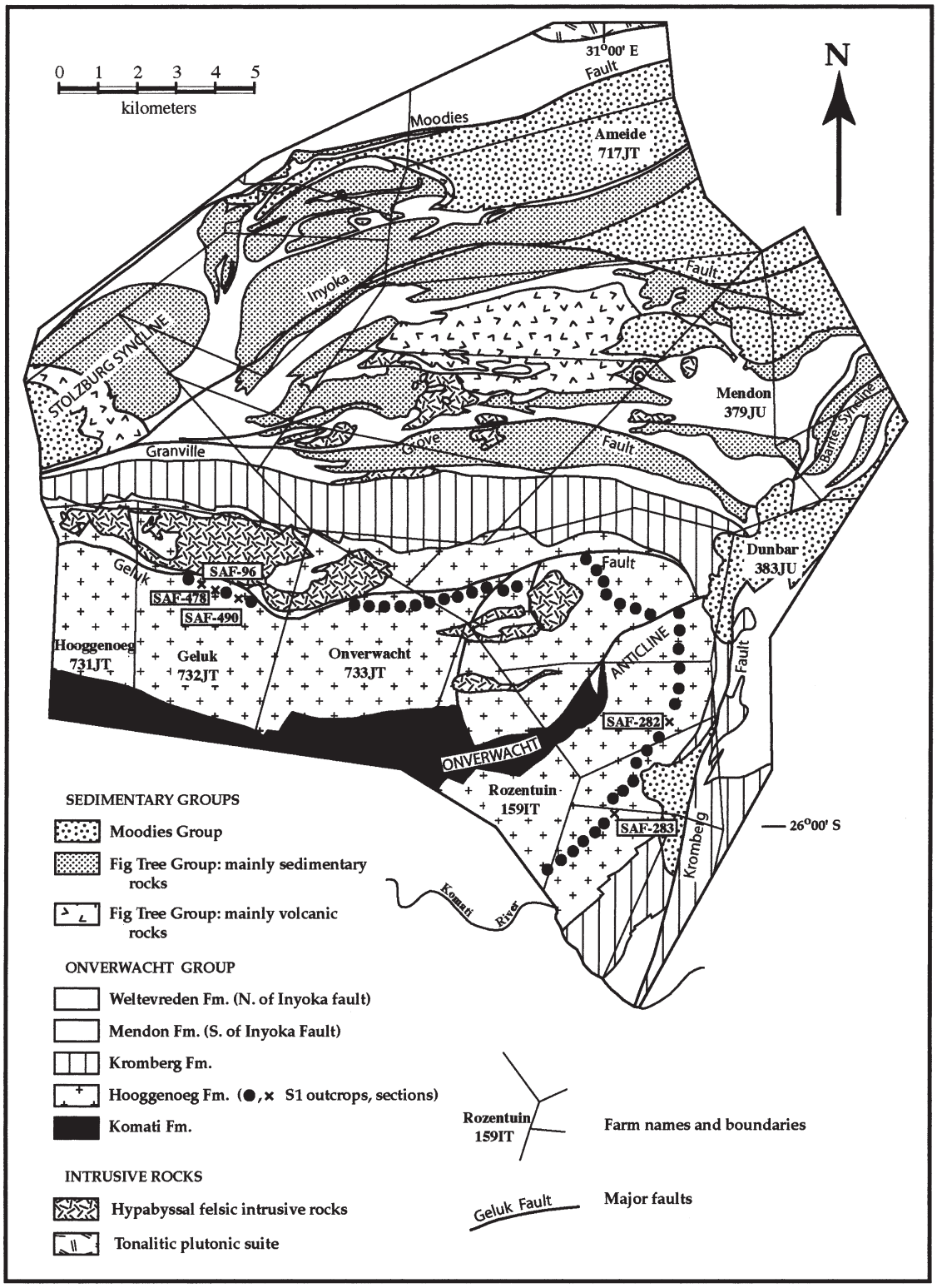

FIG. 3. Geologic map of the west-central part of the BGB. The outcrop of spherule bed S1 is shown by dots, and specific localities discussed in the text and shown in Fig. 4 are designated by locality numbers (Table 1) and the symbol ×. Location of map area shown in Fig. 1. Fm., Formation.

TABLE 1. KEY LOCALITIES OF SPHERULE BEDS S1–S4 IN THE BGB, SOUTH AFRICA

Bed	Location number		Name	Coordinates
	Lowe	*Byerly*		
S1	SAF-96			25°56.28′S, 30°52.68′E
	SAF-283			26°00.32′S, 30°59.92′E
	SAF-337			25°56.10′S, 30°52.23′E
	SAF-478[1]	SA117; SA449		25°56.4′S, 30°52.94′E
	SAF-490	SA526		25°56.6′S, 30°53.84′E
S2	SAF-105			25°54.52′S, 31°03.36′E
	SAF-142-6			25°54.21′S, 30°55.37′E
	SAF-175	SA95		25°54.02′S, 30°59.88′E
	SAF-199			25°54.9′S, 30°55.97′E
	SAF-204			25°54.03′S, 30°58.78′E
	SAF-230			25°54.87′S, 31°03.58′E
	SAF-233			25°54.50′S, 31°02.73′E
	SAF-244			25°54.50′S, 30°54.82′E
	SAF-264			25°53.53′S, 31°00.54′E
	SAF-272,[1] 377	SA312		25°53.78′S, 31°01.09′E
	SAF-275			25°54.47′S, 31°00.93′E
	SAF-372	SA514		25°54.04′S, 31°00.96′E
	SAF-374	SA90		25°54.52′S, 31°01.60′E
	SAF-376			25°53.97′S, 31°01.00′E
S3	SAF-105			25°54.52′S, 31°03.36′E
	SAF-179,[1] 349, 380	SA306, 504	Jay's chert	25°54.9′S, 31°01.13′E
	SAF-227		West Limb Barite Syncline	25°54.44′S, 31°03.68′E
	SAF-295	SA295		25°52.40′S, 30°56.93′E
	SAF-379	SA315	Princeton Tunnel of Agnes Mine	25°50.03′S, 30°58.96′E
	SAF-381	SA323	Sheba Mine	25°42.86′S, 31°08.09′E
	SAF-388	SA346	Stolzburg Syncline	25°52.6′S, 30°53.80′E
	SAF-390	SA344	Mount Morgan Mine overlook	25°50.74′S, 30°55.37′E
	SAF-393		Stolzburg Syncline	
	SAF-294, 296		Florence and Devonian Mine	25°46.21′S, 31°06.11′E
S4	SAF-179,[1] 349, 380	SA306	Jay's chert	25°54.9′S, 31°01.13′E

[1]Denotes type locality.

tion analysis using the Berkeley coincidence–anticoincidence spectrometer. F.T.K. measured Ir by instrumental neutron activation analysis by conventional methods with detection limits of ~1–2 ppb (ng/g). Selected samples were analyzed by radiochemical neutron activation analysis for lower Ir concentrations, and in some cases additional PGEs (Os, Pt, Pd) and Au (Kyte *et al.*, 1992). Methods of Cr isotopic analyses performed by A.S. are described by Lugmair and Shukolyukov (1998).

SPHERULE BEDS

Lowe *et al.* (1989) identified four spherule beds in the BGB: S1 in the upper part of the Hooggenoeg Formation, S2 at the base of the Fig Tree Group, and S3 and S4 within the Fig Tree Group in the southern part of the belt on the west limb of the Onverwacht Anticline. Lowe and Byerly (1999) retained this numbering scheme. However, zircon dating has shown that the Onverwacht–Fig Tree contact is diachronous, ~3,260 Ma in southern areas along the west limb of the Onverwacht Anticline (Byerly *et al.*, 1996) and ~3,243 Ma in the north (Kröner *et al.*, 1991). These results and more recent studies of spherule compositions suggest that S2 is present at the Onverwacht–Fig Tree contact in southern outcrops, where S3 occurs 50–150 m higher in the Fig Tree Group, and that a younger bed, which we correlate with S3, marks the Onverwacht–Fig Tree contact in northern areas. This correlation and numbering scheme is used here (Fig. 2).

Bed S1

Distribution and Lithology. S1 occurs in a 30-cm- to 3-m-thick chert unit, H4c of Lowe and Byerly (1999), in the upper part of the Hooggenoeg Formation (Fig. 2). H4c crops out for at least 25 km

QU1

on both limbs and around the hinge of the Onverwacht Anticline (Fig. 3). Rocks of this age are presently unknown elsewhere in the BGB. Zircons in S1 have been dated at 3,470 ± 3 Ma (Byerly *et al.*, 2002).

S1 is a bed of medium- to coarse-grained current-deposited sandstone, 10–35 cm thick, interbedded with fine-grained tuffs and black or black-and-white banded cherts (Fig. 4). In sections where H4c is <100 cm thick, S1 generally rests directly on or just a few centimeters above altered basaltic to komatiitic volcanic rocks (Figs. 4 and 5). In the type section (SAF-478 in Figs. 3 and 4), H4c is 2.8 m thick, but varies from <50 cm to 6 m thick within 500 m along strike. In this section, S1 is underlain by up to 160 cm and overlain by 90 cm of pale greenish to light gray sericitic chert, black carbonaceous chert, and

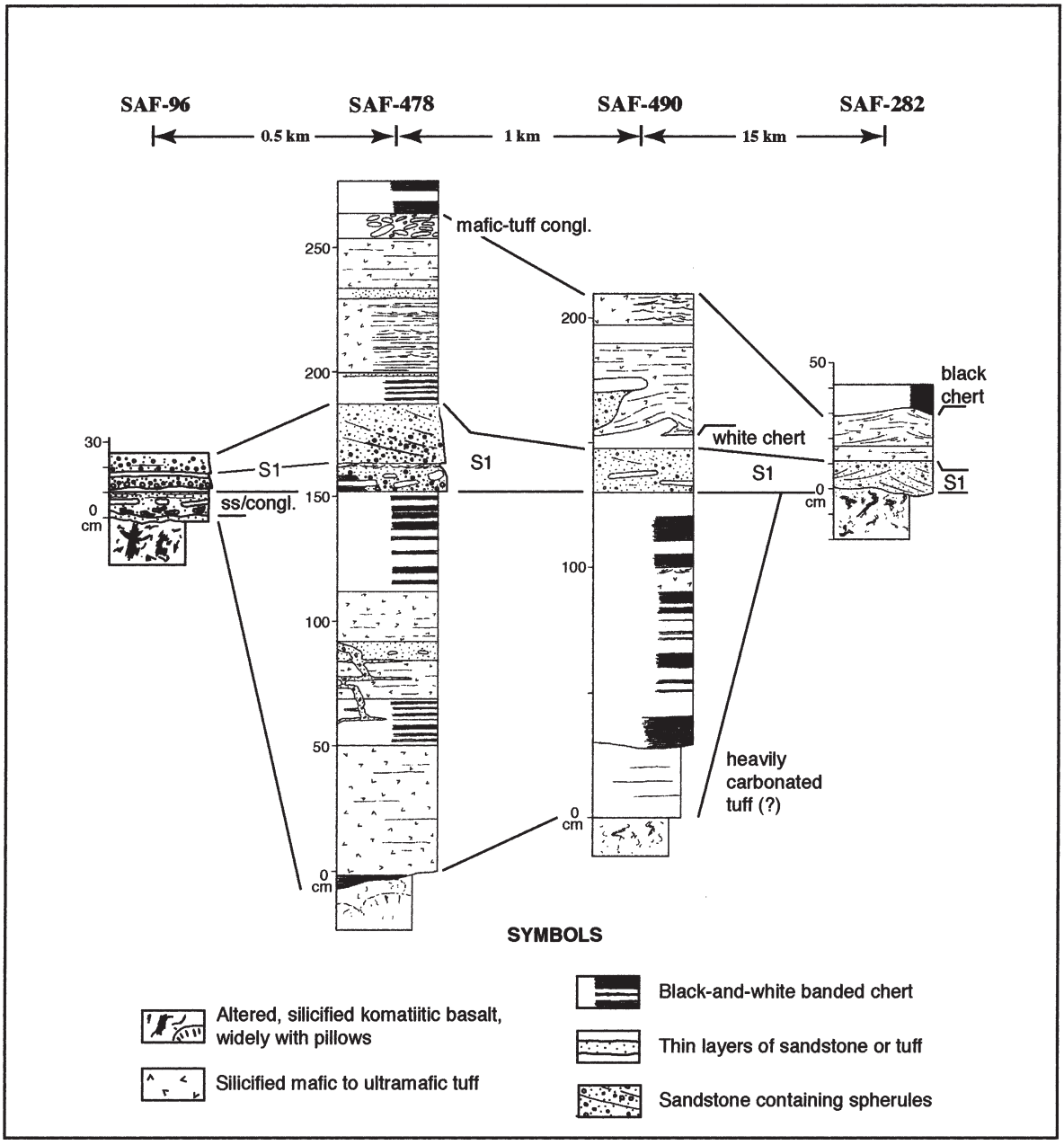

FIG. 4. Stratigraphic sections of chert unit H4c (Lowe and Byerly, 1999) showing the main lithologies and position of spherule bed S1. Note the rapid changes in thickness of H4c over a short distance on the west limb of the Onverwacht Anticline. congl., conglomerate; ss, sandstone.

black-and-white banded chert (Fig. 4) representing silicified fine-grained pyroclastic, biogenic (carbonaceous cherts), and chemical sediments. It consists of two distinct spherule-bearing layers (Figs. 4 and 5A). The lower, S1a, is 10–15 cm thick and composed of normally graded coarse- to medium-grained sandstone containing 10–30% spherules. The base is erosive at least 5 cm into underlying black-and-white banded chert, and the bed contains ripped-up plates and chunks of both black and white chert (Fig. 5A). Spherules and sand grade upward into fine-grained muddy sediment showing cross-lamination (Fig. 5A). The overlying layer, S1b, ~20 cm thick, is also graded and composed of well-sorted, medium-grained sandstone containing 10–20% spherules. It shows low-angle large-scale cross-stratification (Fig. 5A). In sections where S1 rests directly on underlying altered volcanic rocks (Fig. 5B), it consists of 10–30 cm of current-deposited medium- to coarse-grained sandstone containing 1–10% spherules and clasts of chert and altered basaltic volcanic rock.

Ir Content and Cr Isotopic Analysis. Measured Ir levels in S1 lie between 0 (below detection limits) and 3 ppb, with several values around 1.0–1.5 ppb (Table 2). Compared with most sedimentary units in the BGB (Table 3) S1 shows a slight Ir enrichment. One sample from an underlying komatiitic volcanic unit showed 2.1 ppb Ir, still somewhat below that in S1. S1 lacks chrome-rich spinels, which are correlated with elevated Ir levels in S3. No Cr isotopic analyses have been performed on S1 to date.

Spherules. In the type section of S1, spherules are small, ranging from 0.10 to 1.0 mm in diameter, with most in the range of 0.30–0.60 mm (Fig. 6). They range in shape from spheres to ovoids (Fig. 6A), with most having *a/b* axial ratios <2. Some ovoid spherules have maximum diameters in thin section as long as 1.2 mm. The spherules range in composition from virtually pure fine-grained quartz (Fig. 6B–E) to nearly pure sericite, but the latter are uncommon. Where present, they show nearly pure, structureless sericite interiors coated by a thin layer of silica and an outer thin sericite rim. Silica-rich spherules range from 0.20 to 1 mm in diameter and are composed mainly of fine microquartz with sericite rims (Fig. 6B). The largest silica spherules tend to be somewhat blocky in shape rather than smooth spheroids or ovoids (Fig. 6B). Most spherules are micromosaics of intergrown microquartz and sericite. From 40% to 60% of the spherules have dark rims composed of very fine microcrystalline rutile, which appears virtually opaque because of its fine grain size (Fig. 6C, E, and F). Rims range from faint clouds of dispersed rutile to nearly solid opaque rims (Fig. 6E). Some dark rims show a faint fibroradial structure (Fig. 6G). Some vary in thickness and darkness around the spherules, appearing clotted or clumpy, and often have irregular contacts with the underlying spherule interiors (Fig. 6C and F). Many spherules with rutile rims have knobs, bumps, and projections on their surfaces (Fig. 6F).

A few spherules have relatively pure silica interiors composed of one or a few coarse quartz domains instead of microquartz (Fig. 6C and D). Spherules with quartz interiors all show nearly opaque rims (Fig. 6C and E). A small number show circular interior cavities filled by coarse quartz or sericite (Fig. 6D and H). Rare dumbbell-shaped welded spherules are present. Some spherules show fine rutile grains throughout (Fig. 6H). Spherules in both upper and lower layers are similar.

With the exception of rutile, silica, and/or sericite rims, most S1 spherules are massive. A few show silica pseudomorphs after fine, intergrown, randomly oriented, needle- or lath-shaped crystallites that resemble microlites in mafic volcanic rocks, a texture termed microporphyritic. These tend to contain finely divided rutile throughout the material between the crystallites, which was probably originally glass. Other spherules appear to be layered (Fig. 6G). No spinels, pseudomorphs after barred minerals (olivine?), barite, or apatite has been seen in S1, but tourmaline is relatively common. Broken segments of spherules are common (Fig. 6A). Detrital zircons in S1 have been used to date the unit (Byerly *et al.*, 2002).

Admixed nonspherical particles are well-sorted, often irregular detrital grains, virtually all composed of microquartz and sericite (Fig. 6A). A few show outer rims with included fine rutile, and some have fine rutile throughout. Some of these irregular particles appear to have compositions and textures like those of the spherules and may also represent impact-produced debris. However, most irregular particles are altered detrital grains derived by erosion of underlying volcanic or sedimentary rocks.

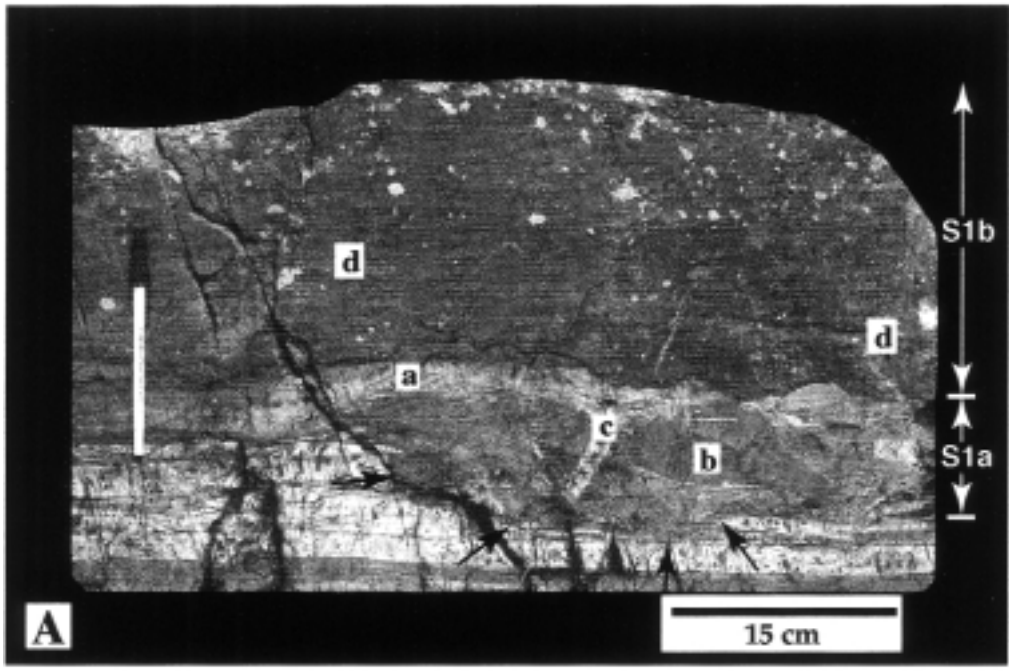
S1b
S1a
d
d
a
c
b
A
15 cm

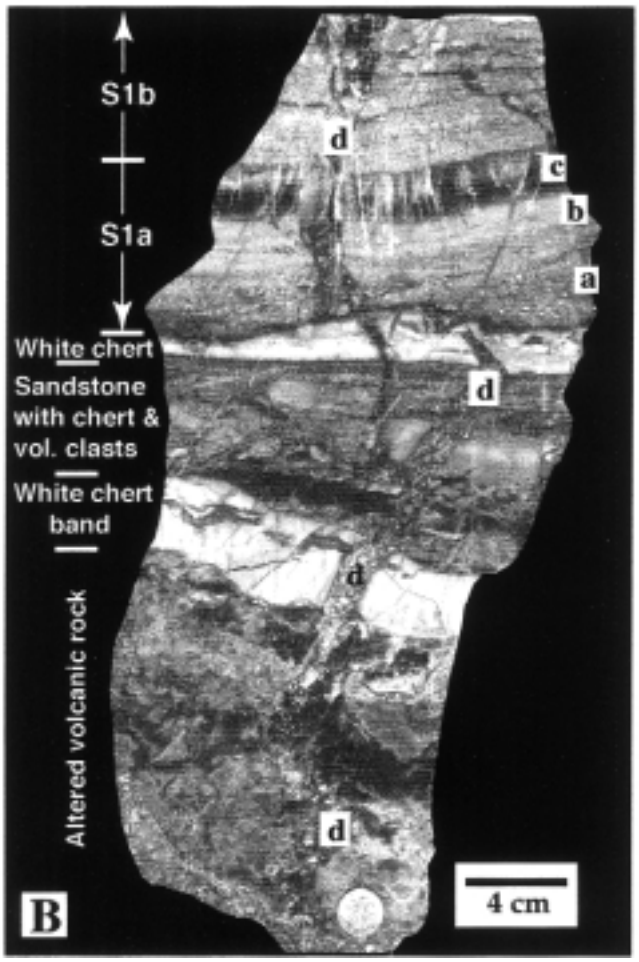
S1b
S1a
White chert
Sandstone with chert & vol. clasts
White chert band
Altered volcanic rock
d
c
b
a
d
d
d
B
4 cm

FIG. 5. Photographs of spherule bed S1. A: Type locality, SAF-478 (Fig. 3). S1 includes two normally graded layers, S1a and S1b, separated by a sharp, probably erosive contact. The top of S1a is marked by small-scale cross-lamination (a). S1a contains rip-up clasts of black (b) and white (c) chert. S1b shows weakly developed low-angle cross-stratification (d). **B:** S1 at locality SAF-96 (Fig. 3). At this locality S1 lies only 5–10 cm above altered volcanic rock and also shows two layers, S1a and S1b. Both show well-developed current structures. S1 is well graded with a lower zone of medium- to coarse-grained spherule-bearing sand (a), an overlying layer of fine silicified sand and silt (b), and a capping layer, now composed of translucent chert, which appears gray in the photograph (c). S1, associated sediments, and the underlying altered volcanic rocks are cut by later chert and debris dikes (d). vol., volcanic.

Sedimentation. S1 is a distinctive coarse-grained, current- or wave-deposited layer within a section of fine-grained biogenic, chemical, and pyroclastic rocks. Overall, H4c was deposited during an interval of low-energy, quiet-water sedimentation marking a widespread period of magmatic quiescence between major eruptive events, represented by the underlying basalts and komatiites of H4v and overlying basalts of H5v (Lowe and Byerly, 1999). Locally, fine black chert at the base of H4c drapes underlying mafic pillows. Although some thin tuffaceous beds show zones of fine cross-lamination, current structures are rare, and large-scale cross-stratification, scour, and coarse detrital units are restricted to S1. The consistency of quiet-water conditions in H4c across its known outcrop suggests that the water was at least moderately deep rather than a localized quiet-water setting within an overall shallow, wave- and/or current-active environment.

Bed S2

Distribution and Lithology. In at least two structural belts on the west limb of the Onverwacht Anticline north of the Granville Grove Fault, the contact between black cherts at the top of the Onverwacht Group and fine ferruginous, cherty, and volcaniclastic sediments of the Fig Tree Group is marked by spherule bed S2 (Fig. 7). S2 has an age of ~3,260 Ma based on an U-Pb zircon age of 3,258 ± 3 Ma on a felsic tuff 20 m above S2 (Byerly *et al.*, 1996). S2 has not yet been identified in more northern parts of the BGB, where correlative rocks include volcanic units or black cherts at the top of the Onverwacht Group (Lowe and Byerly, 1999). The spherule bed at the Onverwacht–Fig Tree contact in the northern BGB, previously correlated with S2, including that at Sheba Mine (Lowe *et al.*, 1989; Kyte *et al.*, 1992; Koeberl *et al.*, 1993), is now correlated with S3 based on zircon dating and spherule compositions.

S2 ranges from ~20 cm to at least 3.1 m thick, and in most sections consists of a low proportion of spherules (<10%) mixed with silt to cobble-sized cherty detritus eroded from underlying volcanic and sedimentary rocks (Fig. 8). In the type section, SAF-272 (Fig. 9), S2 is 3.1 m thick and includes 30–50% spherules.

In most sections, S2 is a compound unit that includes at least two graded layers separated by a surface of erosion or, locally, by thin beds of finer-grained sediment. In the type section, the lower layer is 95 cm thick (Fig. 9). The lower 75 cm consists of displaced and rotated blocks up to 30 cm across of black-and-white banded chert in a matrix of finer cherty grains and very coarse-grained sand-sized sediment containing 30–50% spherules. The top 10–20 cm is medium- to coarse-grained sandstone containing ~10% spherules and showing current structures. This is capped by 25 cm of gray chert representing silicified fine-grained sand, silt, mud, and organic material lacking spherules. The overlying upper unit is 190 cm thick and composed of silicified, mainly coarse- to very coarse-grained chert-grit sandstone containing ~30% spherules and abundant 2–4 cm-long chert clasts (Fig. 9). Zones with current structures are common. It is divided into at least four and perhaps more divisions by 1–2 cm-thick layers of gray chert that represent silicified fine-grained sand, silt, mud, and organic materials. S2 is overlain directly by poorly silicified, finely laminated, banded ferruginous chert of the Fig Tree Group.

To the south, across at least two major faults, S2 at SAF-374 is ~150 cm thick and includes two graded divisions (Fig. 9). The lower is a normally graded unit 90–130 cm thick that includes 5–40 cm of chert- and komatiite-clast breccia at the base, which is locally scoured into underlying chert units, passing upward into 90 cm of current-deposited, coarse- to fine-grained chert-grit sandstone containing <10% spherules. This unit is overlain by 40 cm of chert-plate conglomerate capped by 5–8 cm of sandstone.

TABLE 2. IR AND CR ANALYSES FROM IMPACT LAYERS S1–S4 IN THE BGB, SOUTH AFRICA

Bed, sample number(s)	*Ir (ppb)*[1]	*Ir analytical method*[1]	*Cr (ppm)*
S1			
SAF-96-1[2]	1.5		450
	1.7		509
SAF-283-1[3]	1.2	RNAA	560
SAF-337-1	0.669 + 0.4/−0.3		492
SAF-478-11[4]	3	INAA	535
	0.5	RNAA	535
S2			
SAF-105-23	1.61 + 0.6/−0.5		808
SAF-142-6	3.6 ± 0.6		
SAF-175-7	2.8 ± 0.5		
SAF-175-9	3.9 ± 0.4		
SAF-199-4	1.37 ± 0.18		
SAF-199-5	0.89 ± 0.14		
SAF-199-6	1.38 ± 0.19		
SAF-204-1	0.36 ± 0.17		
SAF-230-1	0.82 + 0.4/−0.3		
SAF-230-4	0.0 + 0.2		
SAF-233	0.0 + 0.2		
SAF-244-3 (base S2)	0.15 + 0.3/−0.1		444
SAF-244-4 (middle)	0.21 + 0.3/−0.1		317
SAF-244-5 (upper)	0.10 + 0.2/−0.1		202
SAF-244-7 (top)	0.10 + 0.2/−0.09		442
SAF-264	0.0 + 0.2		
SAF-275-2-2 (base S2)	0.38 + 0.3/−0.2		210
SAF-275-3 (middle)	1.46 + 0.5/−0.4		266
SAF-275-4 (upper)	2.33 + 0.6/−0.5		299
SAF-275-4A (base of sample)	1.7	INAA	195
SAF-275-4B	3.7	INAA	121
SAF-275-4C	6.1	INAA	161
SAF-275-4D (top of sample)	2.5	INAA	596
SAF-372	0.0 + 0.2		
SAF-374	0.0 + 0.2		
SAF-376	0.0 + 0.2		
S3			
Jay's chert (SAF-179, 349, 380, SA306)			
SAF-179-15	162 ± 6.0		
SAF-349-3	52.7 ± 2.3		568
SAF-380-1 (top)	67.6 ± 3.4		
-2	179 ± 6		
-3	161 ± 4		
-4	100 ± 3.2		
-5 (bed base)	346 ± 11		
SAF-380-5A (sample base)	470	INAA	2,199
-5B	519	INAA	2,446
-5C (top)	426	INAA	2,057
SA306-1-1	204 ± 11		
1-2	31 ± 2		
1-3	103 ± 5		
Barite Syncline, West Limb (SAF-105, 206)			
SAF-105-12-3	144.5 ± 5		808
15	11.5 ± 1.6		1,071
18	96.4 ± 4.1		896
SAF-206-1	2.5 ± 0.5		
2	2.0 ± 0.4		
3	1.88 ± 0.34		
	1.22 ± 0.21		
10	4.5 ± 0.8		239
12	2.3 ± 0.6		204
Barite Syncline, East Limb (SAF-227)			
SAF-227-3	5.8 ± 0.9		488

Florence and Devonian Mine (SAF-294, 295)			
SAF-294-1	66.6 ± 3.4		662
	64.2 ± 1.4		
SAF-295-2	75.9 ± 3.4		707
	69.2 ± 4.0		
SAF-295-3-1	213 ± 10		
3-2	124 ± 5		
3-3	92 ± 5		
3-4	151 ± 8		
Agnes Mine, Princeton Tunnel (SAF-379)			
SAF-379-22	2.84 ± 0.1		
23	1.91 ± 0.05		
Stolzburg Syncline (SAF-388, 393)			
SAF-393-4-1	1.33 ± 0.06		
4-6	4.47 ± 0.14		
Sheba Mine (SAF-381)			
SAF-381-10A (base)	133	INAA	1,055
10B	104	INAA	977
10C	223	INAA	1,617
10D	262	INAA	2,240
10E	447	INAA	2,993
10F	654	INAA	2,782
10G[5]	725	INAA	3,665
10H[5]	430	INAA	2,425
SAF-381-11-1	139 ± 5		
11-2	332 ± 13		
Mount Morgan Mine Overlook (SAF-390, SA344)			
SA344-3-1 (base)	1.12 ± 0.12		
3-2	1.52 ± 0.13		
3-3	1.90 ± 0.16		
3-4	12.59 ± 0.68		
3-5 (top)	9.27 ± 0.52		
S4			
Jay's Chert (SAF-179, 349, 380, SA306)			
SAF-179-15[6] (top)	8	RNAA	350
-14	28	RNAA	420
-13	393	RNAA	1,820
-12	450	RNAA	1,930
-11	286	RNAA	1,700
	89	RNAA	
-10	25	RNAA	1,480
	43	RNAA	
-9	97	RNAA	1,450
-8	54	RNAA	1,320
-7	86	RNAA	1,190
-6	27	RNAA	910
-5	82	RNAA	920
-4	241	RNAA	1,630
-3	161	RNAA	1,640
-2	66	RNAA	1,880
-1 (base sample)	259	RNAA	1,600

[1]Unless otherwise indicated, Ir measurements were made by F.A. using the Ir Coincidence Spectrometer (ICS) at Lawrence Berkeley Laboratory, University of California. The ICS measures Ir abundance following neutron activation by determining the coincidence between two γ-rays of ^{192}Ir using twin Ge crystals. Instrumental neutron activation (INAA) and radiochemical neutron activation (RNAA) analyses were made by F.T.K. at the University of California, Los Angeles.

[2]Cut into four chips, two of which yielded measurable values of 1.5 and 1.7 ppb.

[3]One of two chips yielded a value of 1.2 ppb.

[4]Bed cut into 12 chips. Only one yielded measurable value of Ir of 3 ppb by INAA. A different chip yielded 0.5 ppb by RNAA.

[5]10G is from the top of the lower half of S3, sample 10H averages the entire lower half.

[6]Bed slab cut into 15 chips, numbered 1–15 from base to top (Kyte *et al.*, 1992, their Table 3).

TABLE 3. IR AND CR ANALYSES FROM ROCKS INTERBEDDED WITH SPHERULE LAYERS S1–S4, BGB, SOUTH AFRICA

Rock type	*Stratigraphic unit*	*Sample number*	*Ir (ppb)*[1]	*Cr (ppm)*
Hooggenoeg Formation				
Silicified mafic volcanic rock <S1	H4v	SAF-96-4	2.1 (RNAA)	
Silicified komatiitic ash[2,3]	H5c	SA37-3	0.4 + 0.4/−0.2	138
Dacite[2]	H6	SA31-3	0.0 + 0.3	
Kromberg Formation				
Silicified mudstone		SAF-23-314	0.3 ± 0.3	
Mendon Formation				
Silicified komatiitic ash	M1c	SAF-10-12	1.6 ± 0.5	566
Silicified komatiitic ash	M1c	SAF-10-13	0.5 ± 0.3	618
Silicified komatiitic sandstone	M1c	SAF-186-1	0.5 ± 0.4	2,450
Silicified komatiitic ash[2]	M1c	SA17-9	0.0 + 0.3	
Komatiite, high Mg[2]	M2v	SA72-3	1.3 + 0.7/−0.5	1,630
Komatiite, high Mg[2]	M2v	SA72-4	1.3 + 0.7/−0.5	1,747
Komatiite, high Mg[2]	M2v	SA73-2	2.3 + 0.8/−0.6	2,532
Komatiite, low Mg[2]	M2v	SA224-6	0.4 + 0.5/−0.3	1,826
Komatiite, high Mg[2]	M2v	SA224-7	1.3 ± 0.2	2,098
Komatiite, high Mg[2]	M2v	SA224-12	1.2 ± 0.2	1,980
Komatiite, low Mg[2]	M2v	SA224-15	0.6 ± 0.2	1,152
Komatiite, low Mg[2]	M2v	SA224-16	0.3 ± 0.2	951
Silicified komatiitic ash	M2c	SAF-358-1	1.4 + 0.5/−0.4	393
Silicified komatiite	M3v	SA145-1	0.3 + 0.4/−0.2	1,508
Silicified komatiite	M3v	SA163-5	0.2 + 0.4/−0.2	1,141
Silicified ash	M3v(?)	SAF-273-3	0.1 + 0.2/−0.1	
Komatiite, low Mg	M4v	SA107-1	0.5 + 0.5/−0.3	1,420
Komatiite, low Mg[2]	M4v	SA106-1	4.9 + 1.1/−0.9	4,798
Komatiite, low Mg[2]	M4v	SA106-2	1.5 + 0.7/−0.5	4,381
Komatiite, low Mg[2]	M4v	SA115-1	0.18 + 0.4/−0.2	917
Silicified komatiite	M4c	SA278-1	1.6 + 0.7/−0.5	3,520
Silicified komatiite	?	SA285-1	0.09 + 0.4/−0.1	
Silicified komatiite (<SAF-294)	?	SAF-357-6	1.5 + 0.8/−0.6	
Silicified komatiite <S3		SAF-294-2	3.4 ± 0.4	
Spinifex-bearing komatiite	?	SAF-379-28	2.6 (INAA)	
Silicified komatiite	?	SAF-379-18	1.2 (RNAA)	
Komatiitic dike rock[2]		SA96-1	0.4 + 0.5/−0.3	1,768
Black chert <S2		SAF-275-1	0.0 + 0.2	
Black chert <S3		SAF-295-9	0.3 + 0.3/−0.2	
Black chert <S3 (near SAF-294)		SAF-357-9	0.2 + 0.3/−0.2	
Black chert <S2		SAF-105-1	0.09 + 0.2/−0.08	
Black chert <S2		SAF-105-29	0.07 + 0.2	
Black chert <S2		SAF-244-1	0.1 + 0.2/−0.08	
Black chert <S2		SAF-238-1	1.2 + 0.5/−0.3	
Black chert <S3		SAF-381-5	<0.6 (INAA)	
Fig Tree Group, Northern BGB				
Dacite (dike)	Schoongezicht Fm.	SA31-1	0.0 + 0.2	
Dacite[2]	Schoongezicht Fm.	SA53-2	0.0 + 0.3	
Mudstone >S3 (SAF-294)	Ulundi Fm.	SAF-294-5	0.2 + 0.3/−0.1	
Mudstone >S3 (SAF-294)	Ulundi Fm.	SAF-296-5	0.0 + 0.3	
Jasper >S3 (SAF-294)	Ulundi Fm.	SAF-296-3	0.0 + 02	
Sandstone >S3 (SAF-294)	Sheba Fm.	SAF-296-4	0.2 + 0.3/−0.2	
Shale 9 m >S3	Ulundi Fm.	SAF-381-1	<1.5 (INAA)	
Shale 20 m >S3	Ulundi Fm.	SAF-381-20	<1.6 (INAA)	
Sandstone ≈90 m >S3	Sheba Fm.	SAF-381-21	<1.2 (INAA)	
Fig Tree Group, Southern BGB				
Silicified dacitic dike[2]		SA6-6	0.0 + 0.3	
Silicified dacitic ash: 2 m <S2	Mapepe Fm.	SAF-244-2	0.2 + 0.3/−0.1	
Silicified dacitic ash: 0.6 m >S2	Mapepe Fm.	SAF-244-5	0.1 + 0.2/−0.1	
Sandstone: 12–15 m >S2	Mapepe Fm.	SAF-244-6	0.2 + 0.3/−0.1	
Silicified dacitic ash	Mapepe Fm.	SAF-245-1	0.05 + 0.2	
Silicified ash <S2	Mapepe Fm.	SAF-275-1	<0.6 (INAA)	
Black chert >S2	Mapepe Fm.	SAF-275-5	<0.7 (INAA)	
Dacitic ash <S3 (SAF-295)	Mapepe Fm.	SAF-295-5	0.3 + 0.3/−0.2	
Iron formation	Mapepe Fm.	SAF-17-1	0.2 + 0.4/−0.2	

Mapepe Fm.	SAF-17-1	0.2 + 0.4/−0.2	
Barite	Mapepe Fm.	SAF-240-5	0.3 ± 0.3
Gray chert (silicified dacitic ash?)	Mapepe Fm.	SAF-105-5	0.09 + 0.2/−0.08
Gray chert (silicified dacitic ash?)	Mapepe Fm.	SAF-105-8	0.1 + 0.2/−0.08
Gray chert (silicified dacitic ash?)	Mapepe Fm.	SAF-105-30	0.25 + 0.3/−0.2
Gray chert (silicified dacitic ash?)	Mapepe Fm.	SAF-105-31	0.1 + 0.2/−0.08
Silicified sandstone: ≈3 m <S3	Mapepe Fm.	SAF-380-8	0.26 (RNAA)
Silicified sandstone: ≈2.3 m <S3	Mapepe Fm.	SAF-380-9	0.18 (RNAA)
Silicified sandstone: ≈0.3 m <S3	Mapepe Fm.	SAF-380-11	0.22 (RNAA)
Silicified sandstone: 1.5 m >S3	Mapepe Fm.	SAF-380-14	0.12 (RNAA)
Silicified sandstone: 4.0–4.5 m >S3	Mapepe Fm.	SAF-380-18	0.31 (RNAA)
Silicified sandstone: 0.2 m >S4	Mapepe Fm.	SAF-380-21	0.13 (RNAA)

Stratigraphic units are from Lowe and Byerly (1999). Fm., Formation.

[1]Unless otherwise indicated, Ir measurements were made by F.A. using the Ir Coincidence Spectrometer (ICS) at Lawrence Berkeley Laboratory, University of California. The ICS measure Ir abundance following neutron activation by determining the coincidence between two γ-rays of ^{192}Ir using twin Ge crystals. Instrumental neutron activation and radiochemical neutron activation analyses were made by F.T.K. at the University of California, Los Angeles.

[2]Ir abundance measured against a flux monitor of ^{152}Eu.

[3]This sample was erroneously listed as a dacitic tuff in Lowe *et al.* (1989).

On the east limb of the Barite Syncline (Fig. 3), the base of the Mapepe Formation is marked at least locally by a thin spherule bed that we tentatively correlate with S2. This bed is poorly exposed and not well studied.

Ir Content and Cr Isotopic Analysis. Ir analyses of S2 (Table 2) range from below detection limits to 3.9 ppb with an average of ~1.3 ppb. In some sections, S2 shows little or no Ir anomaly relative to adjacent beds, but in others it exhibits distinctly higher levels (Fig. 10). Locally, elevated Ir levels may be associated with reworked komatiitic debris in S2. Cr isotopic analysis of one sample from S2 (SAF-275) indicates the presence of an extraterrestrial Cr component consistent with a carbonaceous chondrite bolide (Kyte *et al.*, 2003). The isotope effect is not as pronounced in S2 as in S3 and S4. This is not surprising because the spherule content, spinel abundance, and Ir concentration in S2 are much smaller.

Spherules. S2 spherules range from 0.15 to 2.5 mm in diameter (Fig. 11). Their present character is strongly dependent on local postdepositional diagenesis and alteration. In SAF-272, the spherules are well preserved and easily distinguishable from the nearly pure chert matrix/cement and associated angular detrital chert grains and clasts (Fig. 11). They were largely protected from postdepositional compaction by early silica cementation and range in composition from nearly pure sericite to nearly pure silica end members. Silica spherules (Fig. 11B) commonly show thin sericite rims, 0.05–0.2 mm thick, often containing fine dark rutile inclusions. The silica interiors are made up of intergrown, coarsely crystalline, blocky to lath-shaped quartz grains. In some spherules, thin sericite septa separate the blocky quartz grains (Fig. 11C). Sericite-rich spherules, which compose ~50% of the spherules, are composed of very fine-grained, microcrystalline to cryptocrystalline sericite containing up to 50% very fine, intergrown microquartz and up to 10% dispersed rutile needles (Fig. 11D and E). Some are massive, but many show rims enriched in fine rutile, and, in a few, the sericite becomes finer toward the outer surface. In zones of compaction and stylolite formation, sericitic spherules have commonly been crushed and deformed (Fig. 11A). Sericite and quartzose spherule types grade into one another through spherules that have interiors composed of isolated patches of blocky quartz grains surrounded by areas composed of fine sericite and microquartz (Fig. 11C). Rare welded and/or dumbbell-shaped types are present (Fig. 11C), and a few spherules may be teardrop- (Fig. 11D) or button-shaped (Fig. 11E). Some spherules show internal randomly oriented needle-like crystal pseudomorphs (Fig. 11F and G), and some have dark rutile rims displaying a fine fibroradial structure (Fig. 11E). Rare spherules are composed largely of apatite (Fig. 11H).

At SAF-374 (Fig. 9), S2 is composed of coarse sandstone containing <1% spherules, which range from 0.15 to 0.6 mm in diameter. They include sericitic and siliceous types, but all silica is in the

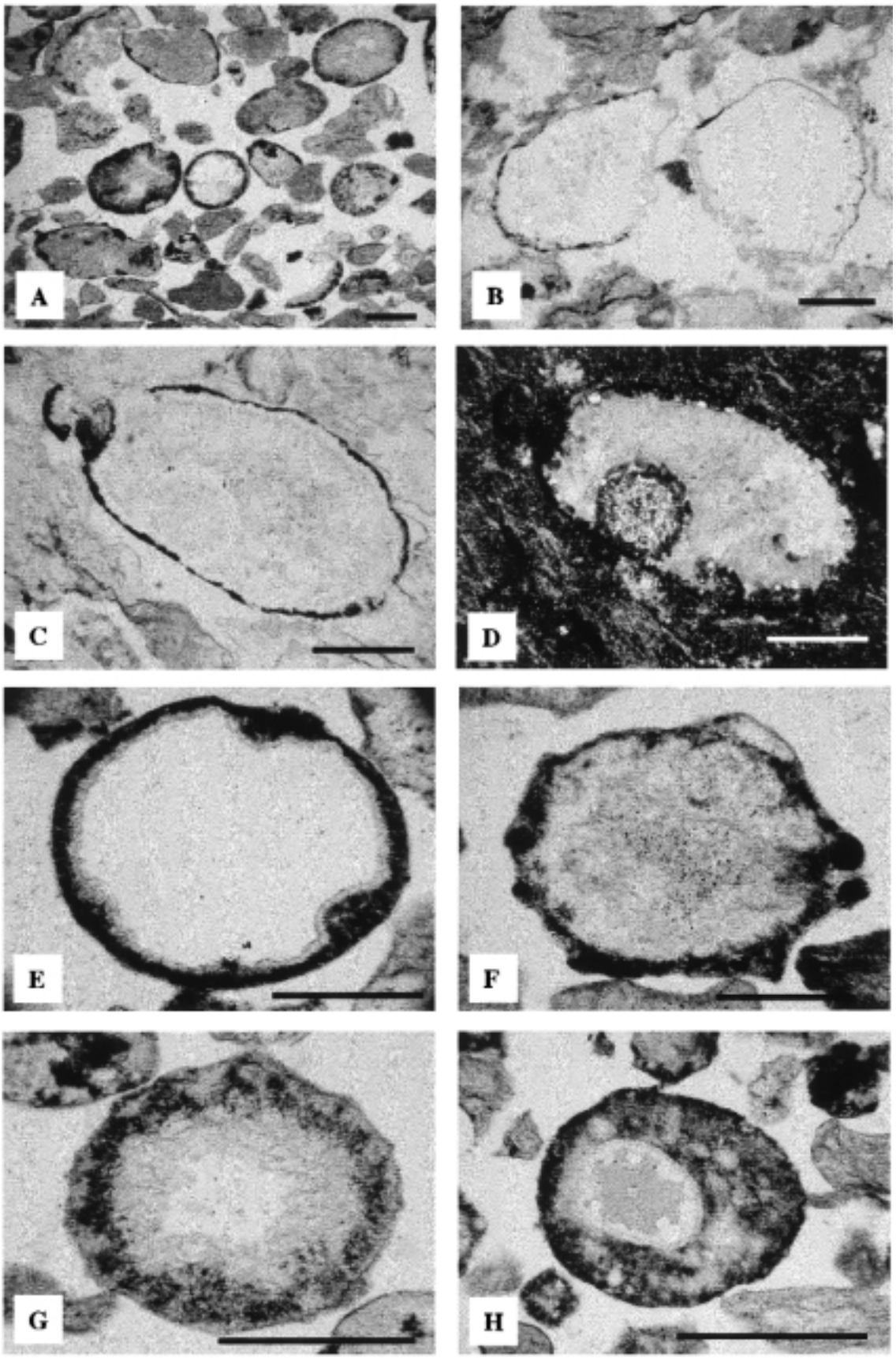
A
B
C
D
E
F
G
H

FIG. 6. Spherules from bed S1 in its type locality, SAF-478. Scale bar is 0.5 mm long in all panels. **A:** General view of S1 showing spherules and associated debris. Note spherule rim segment to left of scale bar. **B:** Pair of large, somewhat irregular, possibly broken silica spherules. **C:** Large silica spherule with a dark rim composed of fine rutile. **D:** Same under crossed nicols (polarizers). The spherule interior consists largely of a single domain (crystal) of coarse quartz (light) rimmed by a <0.1–mm-thick layer of finely crystalline quartz below an outer rutile rim. The spherule also contains an off-centered circular area of fine quartz and sericite representing a filled cavity. **E:** Large silica spherule that includes a dark, nearly opaque outer rim of finely divided rutile and a thin underlying layer of sericite. **F:** Spherule with an interior composed of intergrown quartz and sericite mantled by a rutile-rich rim. The rutile rim is of variable thickness and shows knobs and other irregularities on the surface. A crude fibroradial structure is seen locally at the base of the rim. **G:** Layered spherule with a nearly pure quartz interior (white), a layer of intergrown quartz and sericite (light gray), a zone of intergrown rutile, mica, and quartz (dark), and a thin, discontinuous outer sericite rim. **H:** A small spherule composed of intergrown sericite, rutile, and quartz with a large, off-centered oval-shaped cavity filled with sericite (gray) and quartz (white).

form of very fine microcrystalline quartz that is difficult to distinguish from the cherty matrix. Many spherules have thick rims clouded with fine rutile. In some, variations in the abundance of rutile in the rims outline a crude relict radial or fan-shaped crystal structure. The rims range up to half of the particle radius in thickness. Most spherule interiors are composed of microcrystalline quartz and sericite, often with clumpy masses of microquartz within a sericite-rich matrix. A few spherules have sericite interiors surrounded by a siliceous layer with a dark rim, and many show faint pseudomorphs after randomly oriented lath-shaped crystals. About 20–25% of the spherules show dark, finely divided rutile throughout with variations in rutile abundance outlining altered fine needle- or lath-shaped or barred crystallites. Dumbbell-shaped welded spherules are present.

In addition to quartz, sericite, and rutile, mi-

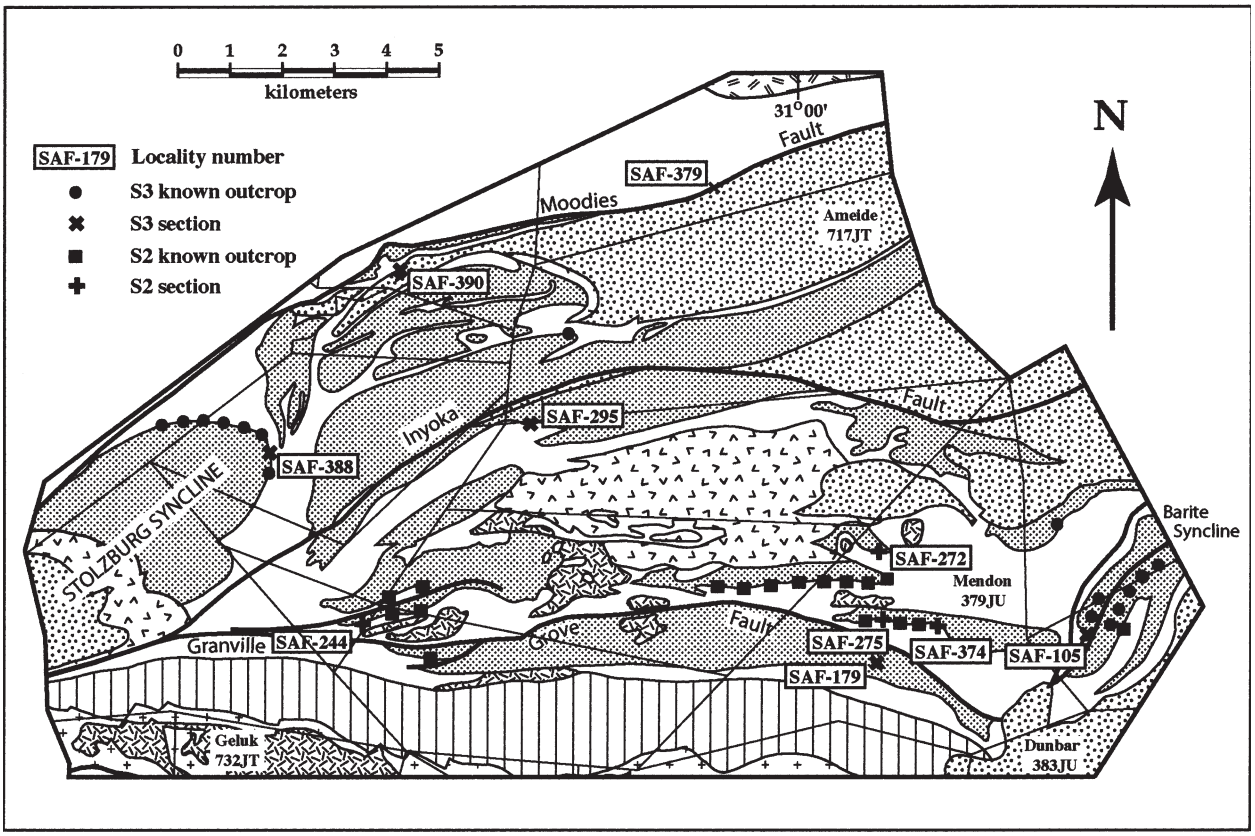

FIG. 7. The principal outcrops and measured sections of spherule beds S2, S3, and S4. Locality SAF-179 is the type locality for both S3 and S4 and the only known locality of S4. Symbols and patterns the same as in Fig. 3.

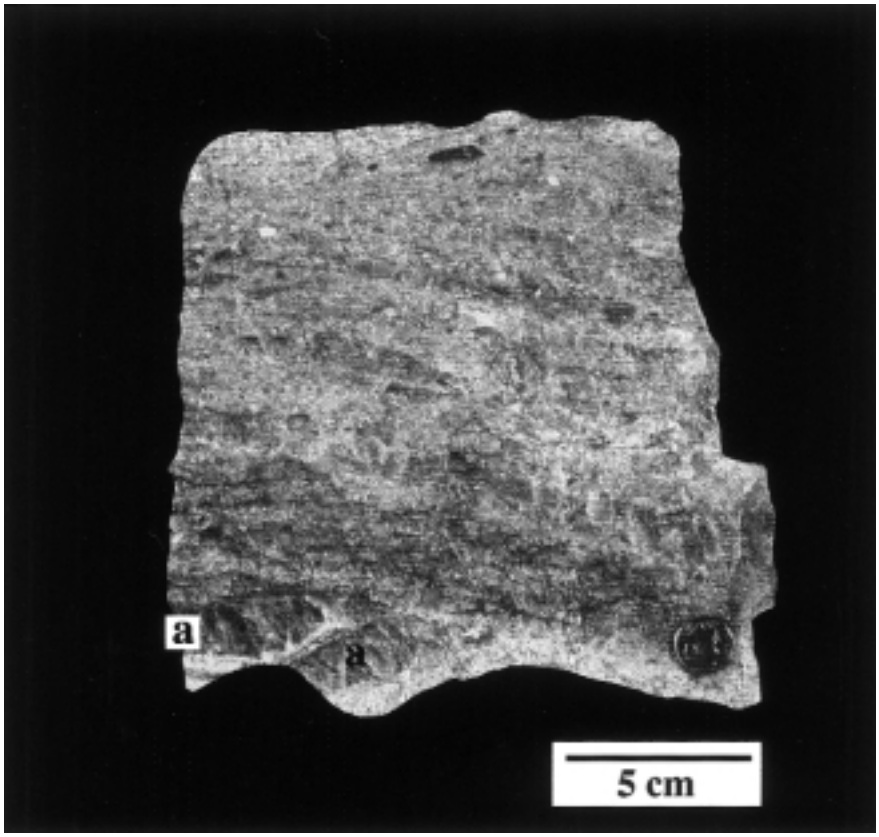

FIG. 8. Photograph of a slab of part of spherule bed S2 showing angular chunks of chert ripped up from underlying units (a) mixed with sand and spherules.

nor amounts of chlorite, barite, apatite, dolomite, pyrite, and chalcopyrite are present in S2. Ni-rich spinels were not seen.

Sedimentation. S2 everywhere shows evidence of deposition by waves and/or currents. It consists mainly of locally derived detritus eroded from underlying Onverwacht cherts and komatiitic volcanic units mixed with spherules. Underlying and overlying units record sedimentation under quiet, low-energy conditions. S2 marks an abrupt, short-lived, high-energy event within otherwise quiet, low-energy, possibly deep-water environments. The presence of multiple, commonly graded sandy layers deposited by highly energetic waves and/or currents separated by breaks or units of fine-grained materials formed by the settling of fine suspended sand, silt, and organic particles indicates that the spherule-depositing event included two or more wave and/or current pulses or events. These were separated by intervals of relatively quiet water during which finer suspended sediment settled and capped the coarser layers. The great thickness of S2 in SAF-272 and the preservation of thin muddy quiet-water layers between thicker wave- and current-deposited units indicate that this was a site of deposition, not erosion, that accumulated sediments stripped off of adjacent, more exposed areas during the high-energy depositional events.

Bed S3

Description and Lithology. S3 is the most widely outcropping spherule bed in the BGB (Figs. 1 and 7). In the southern BGB on the west limb of the Onverwacht Anticline (Fig. 7), S3 is interbedded with terrigenous and tuffaceous sedimentary rocks near the middle of the Mapepe Formation of the Fig Tree Group (Fig. 12). In northern areas, it directly overlies cherts and komatiites of the Weldevreden Formation of the Onverwacht Group and marks the base of ferruginous sediments, banded ferruginous cherts, and locally black cherts of the Ulundi Formation of the Fig Tree Group. In previous reports, this northern bed at the Onverwacht–Fig Tree contact was correlated with S2 (Lowe *et al.*, 1989; Byerly and Lowe, 1994). However, age dating, spinel character and abundance, Ir contents, and spherule types indicate

F12

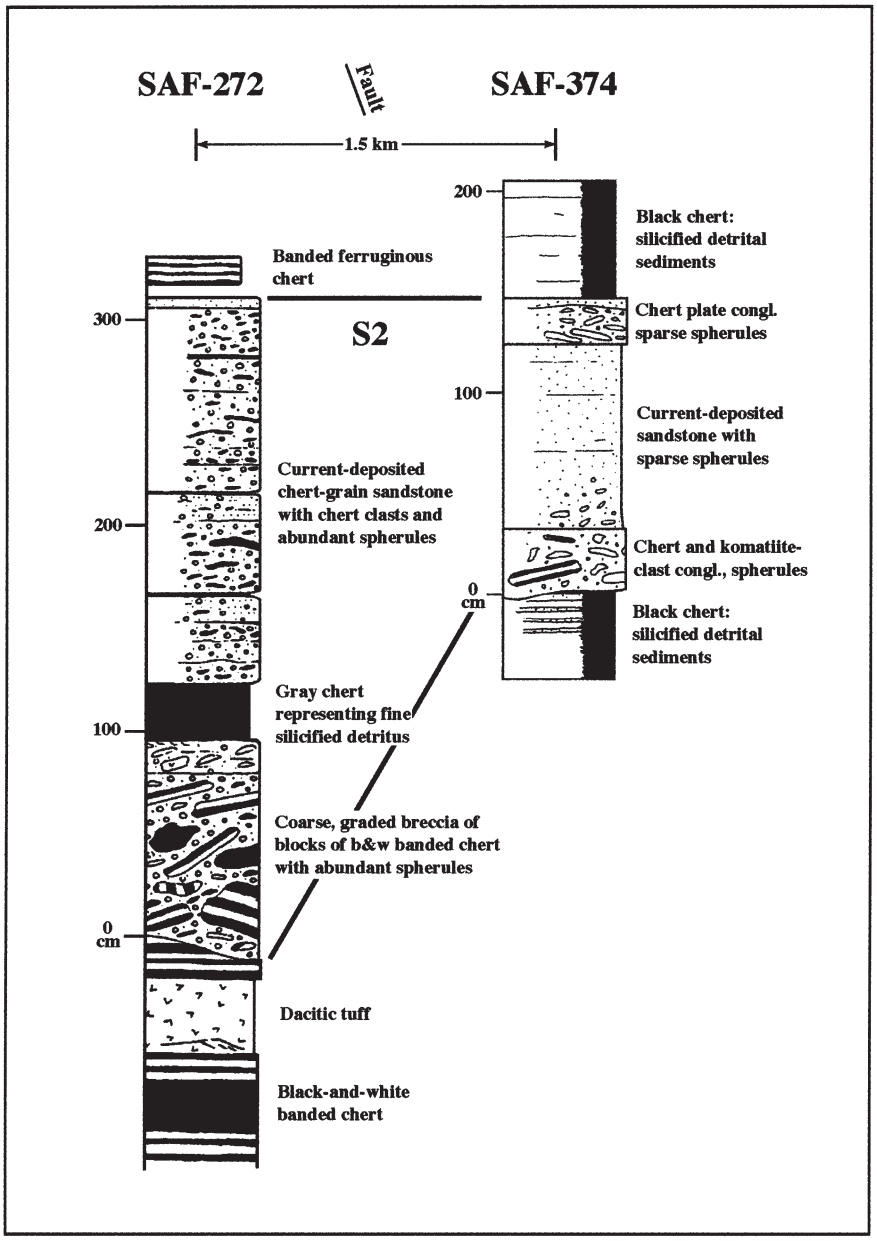

FIG. 9. Stratigraphic sections of S2 and adjacent units at the type locality (SAF-272) and SAF-374. These two localities, only 1.5 km apart, are separated by a major thrust fault. At both localities, S2 is a compound bed composed of at least two normally graded divisions. b&w, black and white; congl., conglomerate.

that this layer correlates with S3 in the southern BGB. S3 varies from 10–15 cm thick in sections affected by shearing and shortening to 2–3 m thick in a few sections where it has been current-deposited. In several sections, S3 shows little or no evidence of deposition by currents, is normally graded, and appears to be a fall-deposited layer (Fig. 13). These sections are generally 30–35 cm thick. An immediately underlying dacitic tuff at SAF-295 (Fig. 7) has been dated at 3,243 ± 4 Ma (Kröner *et al.*, 1991).

In its type section at SAF-179 (Table 1 and Fig. 7), S3 occurs near the middle of a >11-m-thick section of silicified sandstone, mudstone, and intraformational conglomerate called Jay's chert, which lies 100–150 m above the base of the Mapepe Formation (Lowe and Nocita, 1999, their Fig. 3, column F). S3 is at least 78 cm thick in this section, but the base is not exposed (Fig. 12). On the east limb of the Barite Syncline (Fig. 7), S3 occurs 130–150 m above the base of the Fig Tree Group (Lowe and Byerly, 1999, their Fig. 13), where it is 15–40 cm thick, is interbedded with current-deposited tuffaceous sandstone, and shows evidence of deposition by tidal currents. It is present on the west limb of the syncline (Fig. 14, SAF-

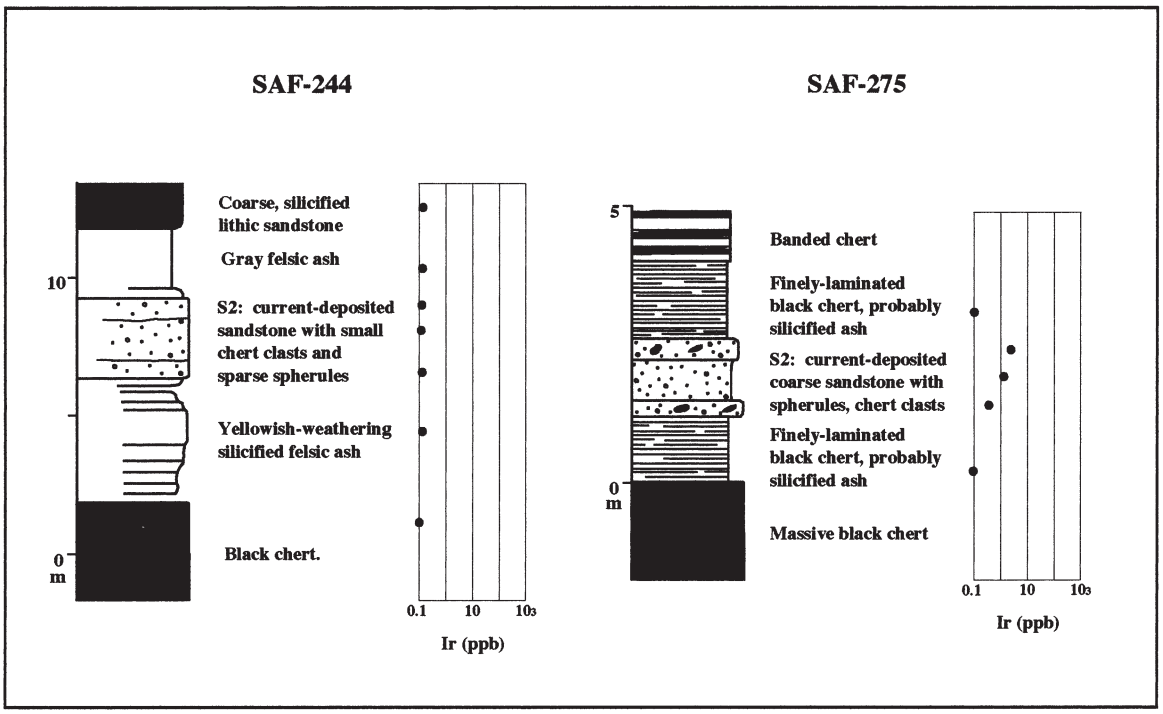

FIG. 10. Stratigraphic sections of S2 and adjacent rocks showing Ir distribution. In both sections, spherules make up <5% of S2. Localities shown in Fig. 7.

105), 10–30 m above the base of the Mapepe Formation, which here rests unconformably on gray to black cherts of the Onverwacht Group. Another key section in the southern BGB, SAF-206, discussed by Lowe and Byerly (1986, their Fig. 2) and Lowe *et al.* (1989, their Fig. 2) is under study by A.K. and will be described in detail in a future paper.

Underground exposures in the Sheba Mine (SAF-381, Fig. 1, locality 2) provide a type section for S3 in the northern BGB, although rocks in this area have been affected by shearing (e.g., Reimer, 1983), and S3 is only 15–20 cm thick. A comparable but poorly accessible surface section is present at the Florence and Devonian Mine (Fig. 14, SAF-294, 296) at the south end of the Ulundi Syncline (Fig. 1, locality 1). S3 also occurs in the Princeton Tunnel of the Agnes Mine (Fig. 7, locality SAF-379).

Ir Content and Cr Isotopic Analysis. Ir contents of S3 vary widely. In the Sheba Mine (SAF-381), where S3 has been thinned by shearing and consists almost entirely of spherules and spherule debris, a 7-cm interval, representing the lower part of the 17-cm-thick bed, was analyzed at 1-cm intervals, yielding Ir concentrations ranging from 104 to 725 ppb (Table 2). In SAF-179, where

FIG. 11. Spherules from bed S2 at SAF-272. Scale bar is 0.5 mm long in all photos. **A:** General view of S2 showing abundant sericite-rich spherules, most with dark rutile rims and many showing the effects of crushing, mixed with angular locally eroded, commonly cherty debris. **B:** Three silica-rich spherules composed largely of coarse blocky quartz. The middle spherule shows an extremely irregular, possibly corroded surface. **C:** Dumbbell-shaped particle formed by the welding of two spherules. The right spherule shows an interior now composed of blocky-quartz grains, each coated by a fine rim of sericite. The left spherule consists of subequal amounts of blocky quartz and patchy sericite. The entire particle has a sericite rim containing sparse fine rutile. **D:** Pair of sericite-rich spherules. Left spherule has a thick, nearly opaque rutile rim as well as isolated rutile grains scattered through interior. It is broken on the left side and may have been more teardrop-shaped when whole. Right spherule has sparse rutile layer that defines a crude barred or fibroradial texture. **E:** Small button-shaped spherule with thick rutile-rich rim overlying a sericite and quartz interior. The rim shows fine relict fibroradial structure. **F:** Small spherule showing pseudomorphs after microlitic crystallites, perhaps originally pyroxene or feldspar. **G:** Small spherule showing fine rutile and relict needle-like crystalline texture throughout. **H:** Spherule composed largely of fine apatite intergrown with rutile.

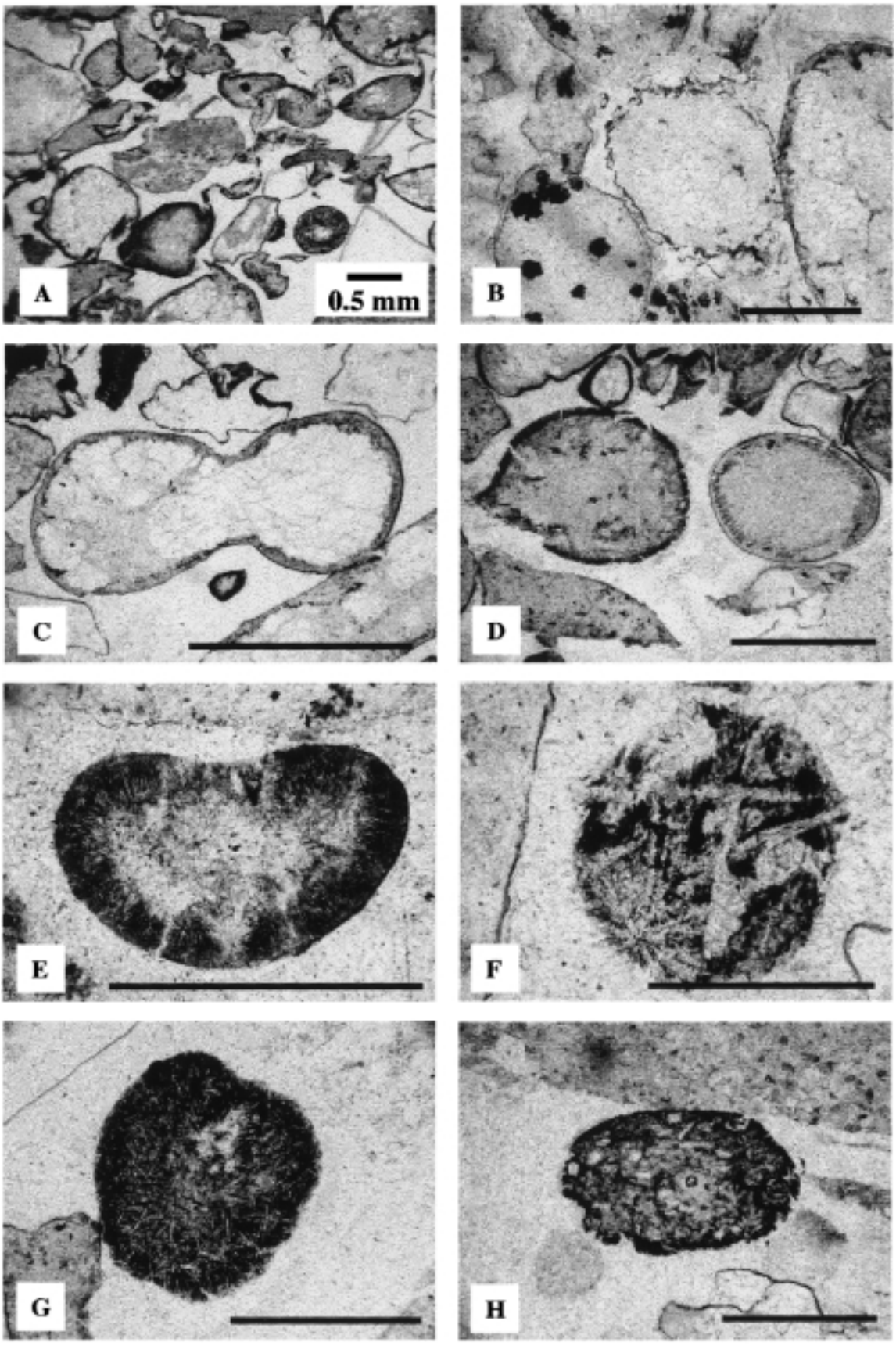
A
0.5 mm
B
C
D
E
F
G
H

spherules make up from 10% to >50% of the rock and are mixed with current-deposited terrigenous detritus, measured Ir from three samples ranges from 426 to 519 ppb (Table 2 and Fig. 12). On the east limb of the Barite Syncline (SAF-227, Table 2) and in the Stolzburg Syncline (SAF-393 and SAF-388), where spherules have also been reworked by currents and mixed with terrigenous and pyroclastic materials, measured Ir abundances in S3 are generally <5 ppb, but in SAF-105 on the west limb they reach >100 ppb (Table 2 and Fig. 14). At the Mount Morgan Mine overlook (SAF-390), where the bulk of S3 consists of nearly undiluted spherules and only the upper part shows current structures, measured Ir ranges from 1.1 to 12.6 ppb, with the highest levels in the upper cross-stratified part of the bed.

Cr isotopic analyses of S3 (Kyte *et al.*, 2003) imply that essentially all Cr in the samples studied is extraterrestrial and indicate a carbonaceous chondrite-type source, most likely a CV-type projectile.

Spherules. Where undisturbed by later waves or currents, S3 is composed entirely of spherules and spherule fragments (Fig. 13). S3 spherules range in size from section to section, but where current working has not extensively size-fractionated the particles, they range from ~0.1 mm to as large as 4 mm in diameter (Fig. 15). At SAF-179, they range from 0.2 to >2 mm in diameter (Fig. 15A). In the Barite Syncline, some spherules reach 4 mm in diameter (Lowe and Byerly, 1986). Spherules between ~0.6 and 1.5 mm in diameter are equally common (Byerly and Lowe, 1994, their Fig. 6).

F15

S3 spherules are commonly preserved as essentially spherical grains, especially where cemented by silica (Fig. 15B). In some sections, more micaceous spherules show effects of crushing and compaction more than associated silica-rich spherules (Fig. 15B) (Lowe and Byerly, 1986), and in many rocks, spherule shapes have been locally modified by pressure solution and stylolite development. In the Sheba Mine spherules in S3 are typically flattened (Reimer, 1983), as are many from the area of the Agnes Mine (Reimold *et al.*, 2000).

S3 displays a variety of spherule types (Fig. 15). In some sections that show little or no evidence of reworking by currents, parts of S3 are composed of a bimodal assemblage of large silica and smaller Cr-rich sericite spherules (Lowe and Byerly, 1986, their Fig. 2). The large silica spherules, 0.1–4 mm in diameter (Fig. 15B), are composed of microcrystalline quartz that commonly shows relict fan-shaped growth or devitrification textures under crossed nicols. They are coated by a thin rim of greenish Cr-rich sericite (Fig. 15B). Admixed smaller spherules, generally 0.4–2.0 mm in diameter, are composed almost entirely of massive Cr-rich sericite (Fig. 15B). Both spherule types commonly have thin (<0.1-mm-thick) opaque rutile-rich rims. In a few sections, such as SAF-179, the phyllosilicate-rich spherules are composed of chlorite.

Other parts of these beds and most current-worked sections, such as at SAF-179, are composed of a mixture of spherule types (Fig. 15A). These include pure silica spherules, most of which are small, <1 mm in diameter (Fig. 15A); larger, nearly pure phyllosilicate spherules (Fig. 15C and D); spherules with phyllosilicate-rich interiors covered by an outer layer of nearly pure silica (Fig. 15A and G); intergrown sericite or chlorite and microquartz spherules; spherules with dendritic and octahedral spinels (Fig. 15A); spherules displaying pseudomorphs after a variety of internal crystal morphologies, including barred minerals (Fig. 15F), probably olivine; edge-centered fibroradial crystals or devitrification textures (Fig. 15E); and lath- or needle-shaped crystals, possibly plagioclase or pyroxene microlites (Fig. 15H). Many show centered to off-centered circular areas of quartz ranging from microquartz to large single-domain quartz masses representing filled cavities (Fig. 15C). Most or all of these varieties are commonly present within individual thin sections, a diversity that emphasizes the heterogeneous composition of the original particles. Future studies are needed to resolve fully which of these textures reflect primary features and components (spinels, barred textures, microlites) and which might have formed during diagenesis and metasomatism.

In addition to quartz, sericite and/or chlorite, and spinel, S3 layers commonly include accessory amounts of apatite, which locally forms up to 60% of individual spherules (Byerly and Lowe, 1994, their Fig. 3d), rutile, barite, diagenetic K- and Ba-bearing feldspar, siderite, and sulfide minerals, including pyrite and chalcopyrite in southern localities and FeNi sulfides in northern localities. In S3 outcrops on the west limb of the Barite Syncline, spherules are widely replaced by barite and have been called barite ooliths (Heinrichs and Reimer, 1977).

Spinels are present in from <1% to a maximum

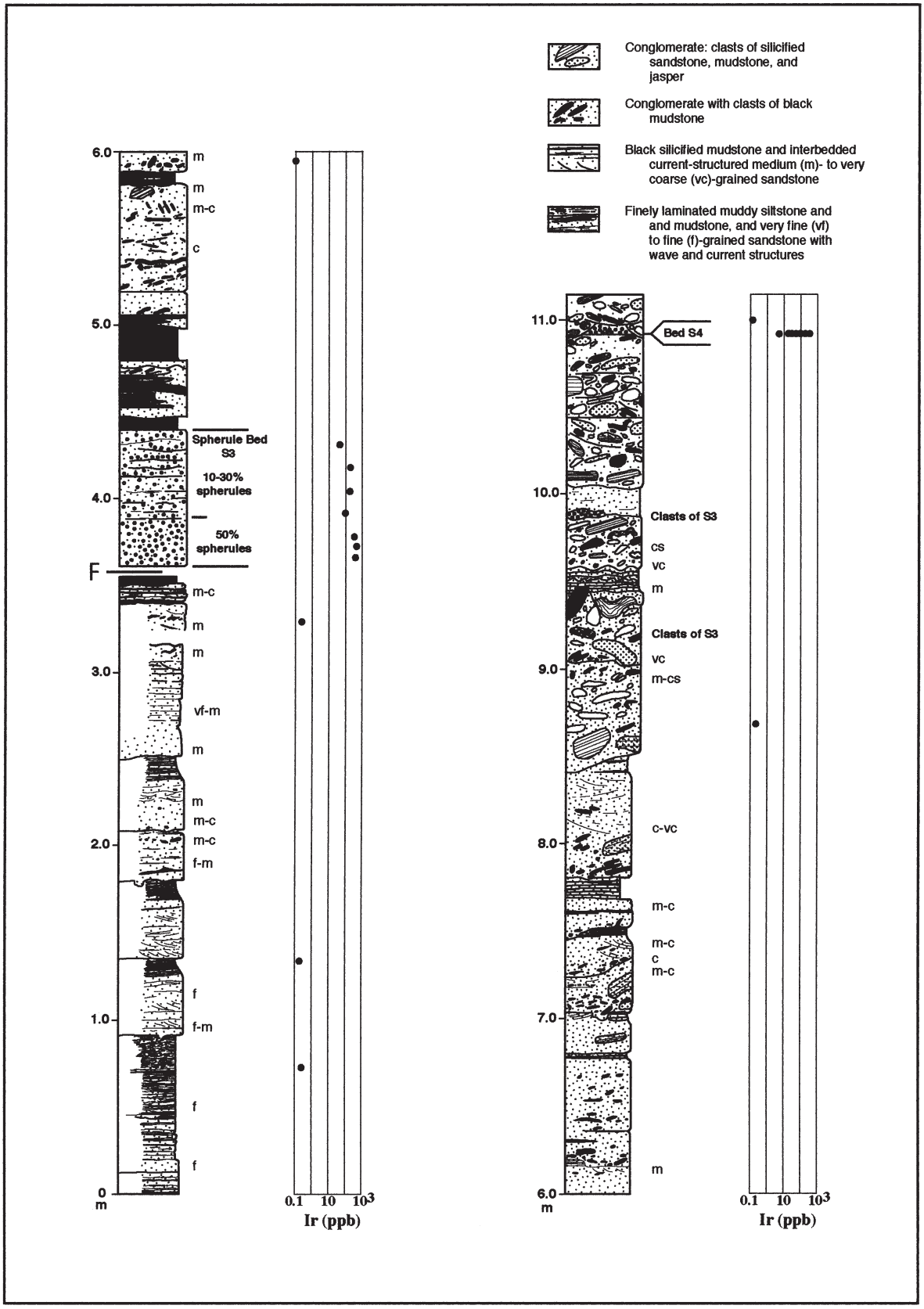

FIG. 12. Stratigraphic section of spherule beds S3 and S4 and associated fan-delta units in their type sections in Jay's chert, SAF-179 (modified from Fig. 13 of Lowe and Nocita, 1999). Ir distribution shown for S3, S4, and adjacent clastic units. c or cs, coarse.

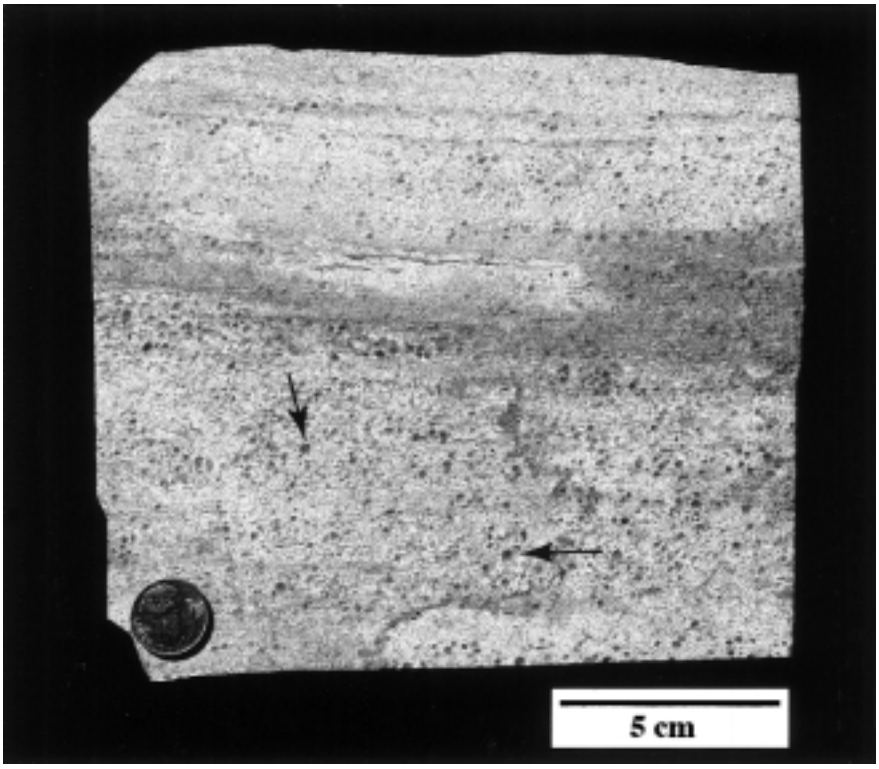

FIG. 13. Slab of part of spherule bed S3 where it consists of nearly pure spherules, including both large, translucent silica (dark, arrows) and sericite-rich (light) types. The fall-deposited bed shows a crude horizontal layering, suggesting variations in texture of falling materials or later weak sorting by waves or currents.

of ~10% of the spherules in S3 (Byerly and Lowe, 1994). They are absent at some localities, especially where the spherules were reworked by currents and mixed with non–impact-produced debris. Spinels within spherules typically show dendritic and skeletal octahedral morphologies (Byerly and Lowe, 1994, their Figs. 3 and 4; Reimold *et al.*, 2000, their Fig. 8). They are similar to those in Cenozoic impact materials, including very high Ni and ferric iron contents, but are distinctive in being composed mainly of chalcophile elements Fe, Ni, Cr, and V. They are unlike spinels in interbedded komatiitic volcanic rocks. Two spinel types are recognized: chalcophile spinels with low MgO, Al_2O_3, and TiO_2; and lithophile spinel with up to 5% Al_2O_3 and MgO. Both types occur in both northern and southern sections. The compositional variability of S3 spinels has been interpreted in terms the initial condensation and subsequent reentry history of particles formed in an impact-produced vapor cloud (Byerly and Lowe, 1994).

Sedimentation. In southern and eastern sections (Fig. 7), S3 was deposited in shallow-water to terrestrial environments. At SAF-179 (Fig. 12), it is interbedded with coarse sandstone and intraformational conglomerate deposited on a small fan delta and shows evidence of current- and/or wave-working and mixing with locally derived terrigenous debris (Lowe and Nocita, 1999). On the east limb of the Barite Syncline (Fig. 7), S3 is interbedded with cross-stratified current-deposited tuffaceous strata, is characterized by large-scale cross-stratification and mixing of spherules with tuffaceous and terrigenous grains, and shows evidence of deposition by tidal currents.

In northern sections (Figs. 1 and 7), S3 was widely deposited under deep-, quiet-water conditions. A series of sections from southwest to northeast along the frontal part of the BGB shows a progressive change from shallower- to deeper-water settings (Fig. 16). At SAF-388 and adjacent outcrops around the hinge zone of the Stolzburg Syncline (Fig. 7), S3 varies from 1 to >2.5 m thick. It includes a lower-graded layer of komatiitic and black chert clasts, 0–1.5 m thick, overlain by current- and/or wave-worked, coarse conglomeratic chert- and komatiite-grain sandstone containing sparse (<5%) spherules. Deposition of S3 in this area involved severe disruption of the sea floor including stripping of any preexisting black cherts or carbonaceous sediments at the top of the

F16

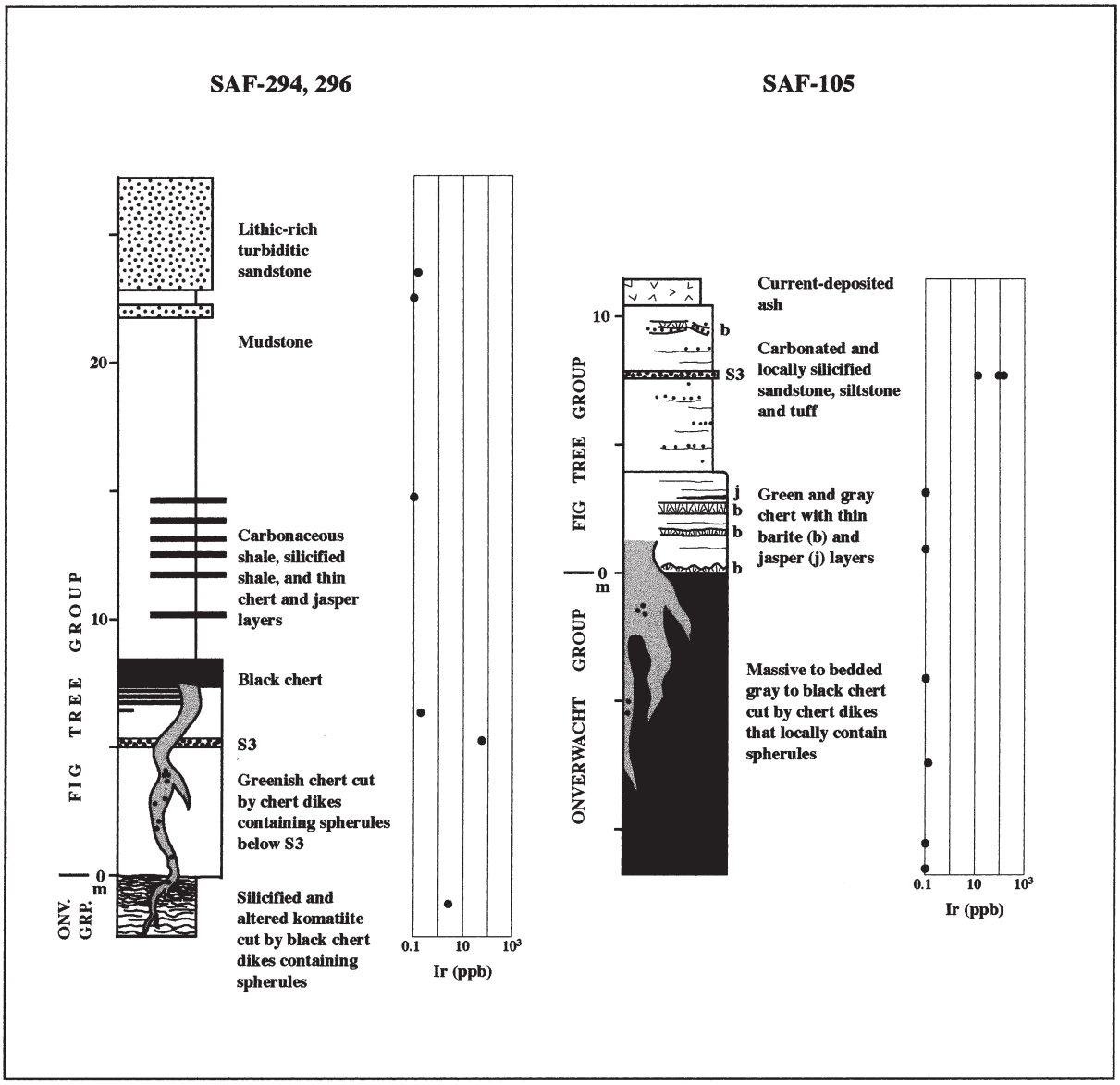

FIG. 14. Ir distribution in S3 and adjacent units at the Florence and Devonian Mine (SAF-294, surface; SAF- 296, underground) in the northern BGB (Fig. 1) and SAF-105 on the west limb of the Barite Syncline (Fig. 7). In both areas, large dikes of black chert that locally contain spherules extend downward into underlying rocks. ONV. GRP., Onverwacht Group.

Onverwacht Group and erosion down into underlying spinifex-bearing komatiitic volcanic rocks. The overlying, regionally extensive Ulundi Formation of the Fig Tree Group (Fig. 2), 20–50 m thick, is composed of fine, laminated ferruginous sediments and chert deposited under quiet-, deep-water conditions. The Ulundi Formation is overlain along the entire northern part of the BGB by the Sheba Formation, a thick sequence of deep-water turbiditic sandstones (Condie *et al.*, 1970). Deposition of S3 at SAF-388 involved a sudden, highly energetic wave and/or current event, erosion of the sea floor, gradual waning of the high-energy event, and progressive deposition of an overall fining-upward graded bed (Fig. 16). This high-energy event was followed by quiet, low-energy, prolonged deep-water sedimentation in early Fig Tree time.

About 4.5 km to the northeast at the Mount Morgan Mine overlook (locality SAF-390, Fig. 7), S3 is 35 cm thick and consists of a lower 20–25 cm composed essentially of undiluted, probably

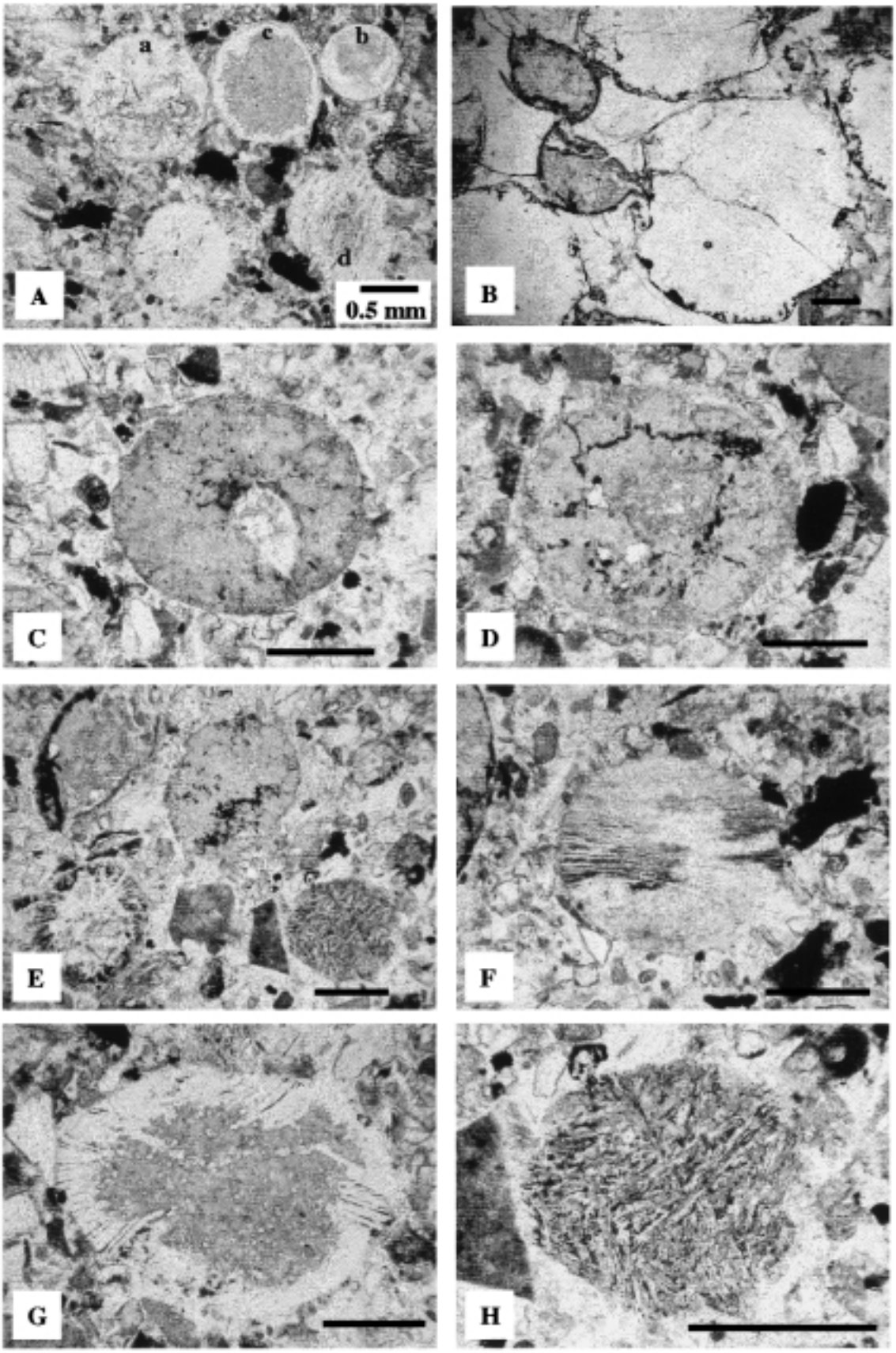
a
c
b
d
A
0.5 mm
B
C
D
E
F
G
H

FIG. 15. Spherules from bed S3. Scale bar is 0.5 mm long in all photos. All photos from SAF-179 except **B**, which is from near SAF-105. **A:** Group of spherules of varied composition including spherule with fine dendritic spinels (a), small nearly pure silica spherule (b), spherule with chlorite-rich interior surrounded by a layer of silica (c), and spherule with faint crystalline, possibly barred texture (d). **B:** Bimodal mixture of large, silica spherules and smaller sericite-rich spherules (left). Sericite-rich spherules show effects of crushing (Lowe and Byerly, 1986) similar to that described by Conley (1977) in oolites. **C:** Large chlorite-rich spherule with off-center, teardrop-shaped patch of quartz thought to represent a filled cavity. **D:** Large chlorite-rich spherule with irregular patches and sheets of rutile (dark). **E:** Group of spherules including nearly pure chlorite spherule (top center) containing patchy rutile and a pair of spherules with pseudomorphs after fine microlitic crystallites. **F:** Spherule with a relict barred texture, probably after olivine. **G:** Spherule with an interior composed of nearly pure chlorite and an outer layer of microquartz showing pseudomorphs after crystalline or possibly barred material. **H:** Spherule showing chlorite, quartz, and rutile after pseudomorphs of microlitic crystallites.

fall-deposited spherules and an upper 10–15 cm containing 30–60% spherules mixed with other detrital components and showing large-scale, current-produced cross-stratification (Fig. 16). At the Florence and Devonian Mine and the Sheba Mine (Fig. 1), 19 and 25 km northwest of SAF-390, respectively, S3 is 15–35 cm thick, but has been thinned by shearing. It is composed essen-

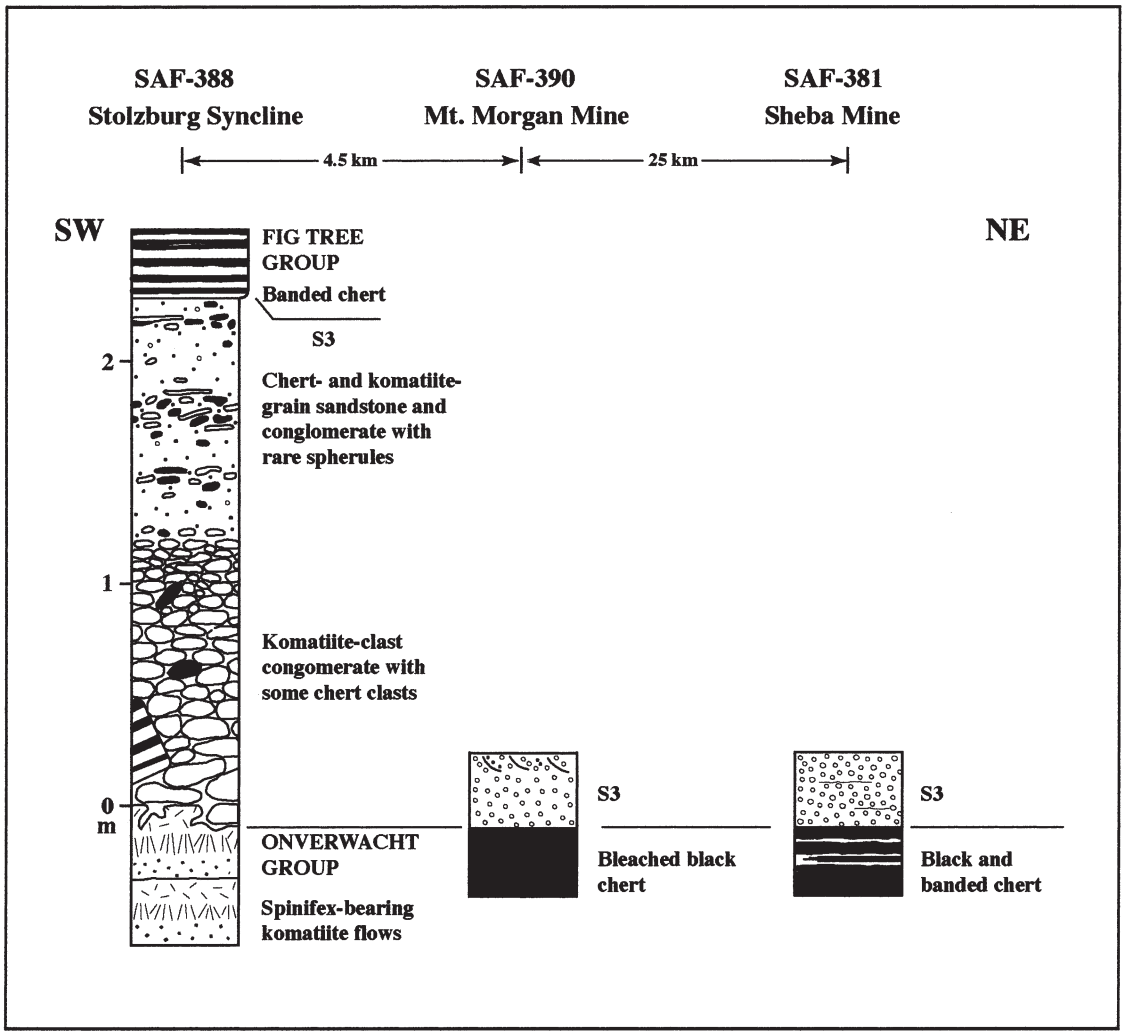

FIG. 16. Sections of S3 along the northern margin of the BGB showing southwest-to-northeast decreasing effects of tsunami-generated waves and currents in reworking fall-deposited impact debris and eroding underlying chert and volcanic rocks. This change is interpreted to reflect progressively deeper water settings of deposition from southwest to northeast. Line of sections extends from the east end of Stolzburg Syncline (SAF-388, Fig. 7) for 30 km to the northeast to the Sheba Mine (Fig. 1, locality 2).

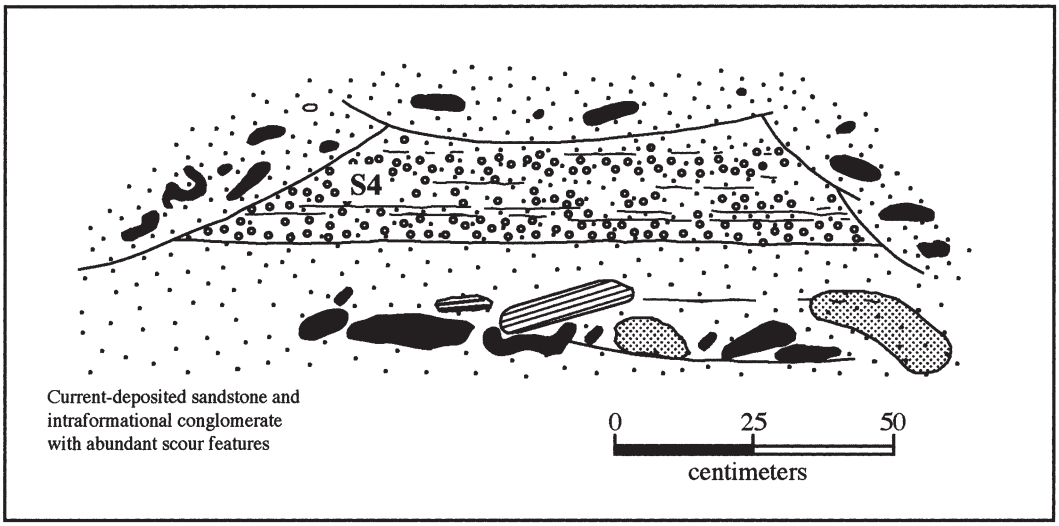

FIG. 17. Sketch of the only known outcrop of spherule bed S4 at SAF-179. The bed is cut out by erosion at the top and along both margins.

tially of pure spherules and spherule debris and lacks evidence of postdepositional reworking by waves or currents. These transitions in S3 over a distance of 25–30 km are interpreted to reflect deposition under progressively deeper-water conditions from southwest to northeast. In the shallowest areas, represented by outcrops in the Stolzburg Syncline, waves and currents accompanying deposition of S3 were effective in scouring the sea floor and briefly transporting coarse eroded detritus and falling impact-produced materials. In deeper-water areas, such as the Mount Morgan Mine overlook, these waves and currents were less effective and moved and transported only the upper part of the fall-deposited sediments and did not substantially erode older sediments or the sea floor. In the deepest waters, represented by S3 in the Sheba Mine, spherules accumulated passively as nearly pure fall-deposited layers with no bed erosion and little or no sediment movement.

Bed S4

Distribution and Lithology. S4 is known from a single outcrop at SAF-179, 6.5 m stratigraphically above S3 (Figs. 7 and 12). The bed crops out for ~1 m along strike and is cut out by erosion beneath units of sandstone and conglomerate within a fan-delta sequence (Fig. 17). It consists of ~15 cm of dark greenish gray current-deposited sandstone containing chlorite spherules mixed with spherule debris and sparse terrigenous clastic grains. S4 may be widely distributed in the BGB. If so, poor exposure due to deep weathering of Fig Tree rocks prevents its identification. At SAF-179, the upper part of the fan-delta sequence has been silicified, and both S3 and S4 crop out as part of a resistant chert unit called Jay's chert.

Ir Content and Cr Isotopic Analysis. Ir abundances in S4 have been reported by Lowe *et al*. (1989) and in detail by Kyte *et al*. (1992), and commonly reach 250–350 ppb (Table 2). The highest measured value from our studies is 450 ppb. Kyte *et al*. (1992) also analyzed Pd, Os, Pt, and Au in S4. Os/Ir and Pt/Ir ratios showed values ~80% of those of CI chondrites. Pd/Ir and Au/Ir were 40% and 2% of CI chondritic values, respectively, indicating substantial fractionation, most probably attributable to differential element depletion during regional metasomatic alteration. Spinels have not been detected in S4, and the PGE carriers remain unidentified (Kyte *et al*., 1992).

The Cr isotopic compositions in two samples from bed S4 are unquestionably non-terrestrial: The $^{53}Cr/^{52}Cr$ ratios are -0.32 ± 0.06 ε and -0.26 ± 0.11 ε (Shukolyukov *et al*., 2000). This confirms the cosmic origin of this spherule bed and suggests a carbonaceous chondrite-type bolide.

Spherules. S4 spherules are composed largely of massive very fine-grained chlorite (Fig. 18). Most

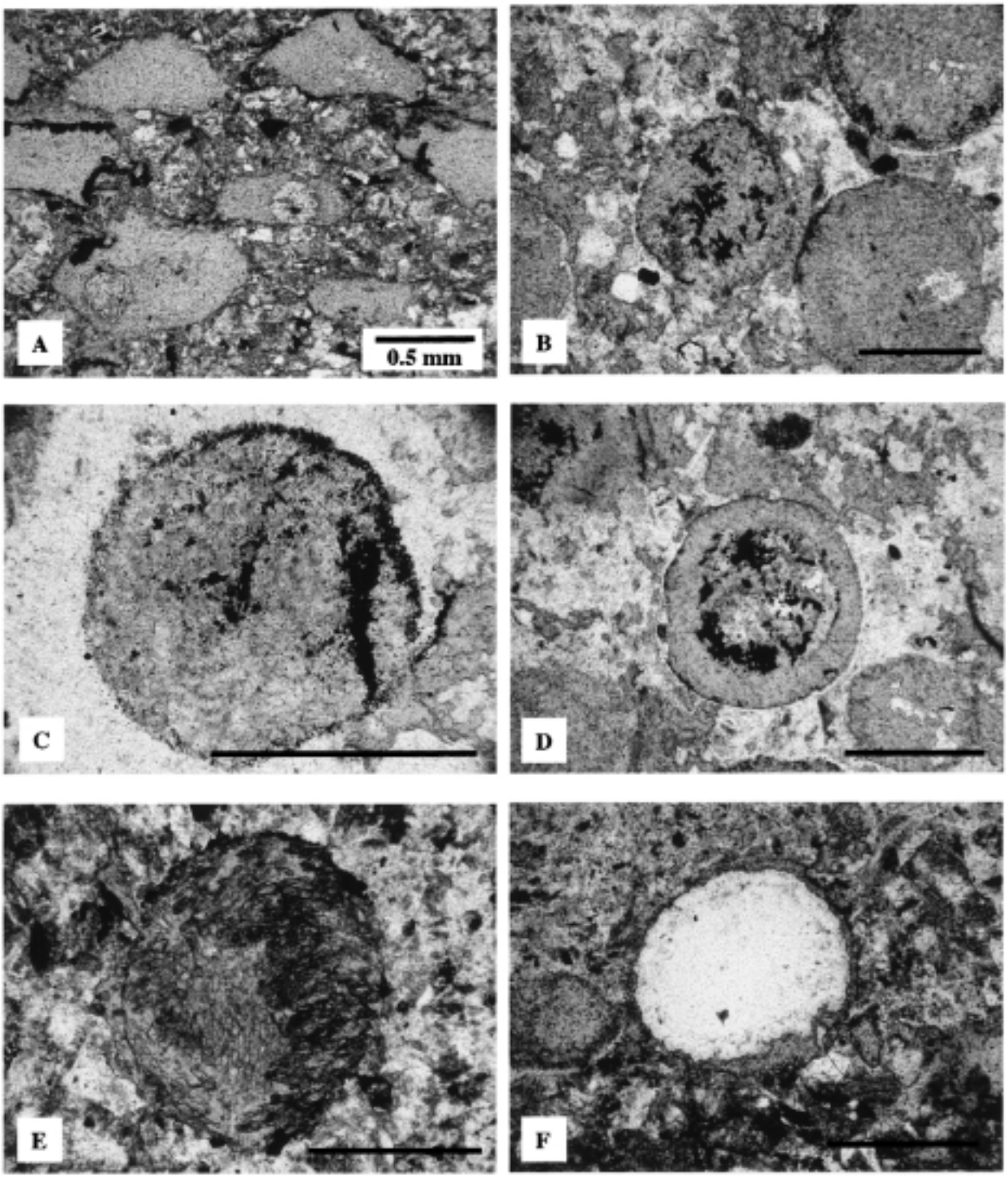

FIG. 18. Spherules from S4 at SAF-179. Scale bar is 0.5 mm long in all panels. **A:** View of flattened chlorite spherules, some with dark rutile rims. Two show internal round structures containing microquartz and chlorite, which are thought to represent filled cavities. The matrix is mostly chlorite-rich debris, but a few clear angular detrital quartz grains are present. **B:** Well-preserved chlorite spherules, one (upper right) with rutile-rich rim and another (center) with irregular patches of disseminated rutile. **C:** Chlorite-rich spherule with patchy rutile. **D:** Layered spherule with chlorite- and rutile-rich interior coated by a layer of nearly pure chlorite. **E:** Chlorite-rich spherule showing an oriented felty fabric, possibly after original crystallites. The two distinct domains with different orientations of chlorite may represent amalgamated liquid droplets. **F:** Unusual silica-rich spherule.

are flattened with *a/b* axis ratios >2 (Fig. 18A). Relatively spherical S4 spherules range from ~0.2 to 1.6 mm in diameter (Fig. 18B–E). Many have disseminated rutile grains or rims containing abundant rutile, up to 25–30% (Fig. 18B–D). A few spherules show layering (Fig. 18D), internal crystalline textures (Fig. 18E), and irregular, sharply bounded areas suggesting the possible amalgamation of originally separate liquid masses (Fig. 18E). One or two spherules are composed largely of quartz (Fig. 18F). Spherules and spherule fragments are mixed with other detrital grains, which now make up from <5% to >90% of individual thin sections. The bulk of this detritus is angular to subangular particles of chert composed mainly of microquartz, but coarsely crystalline quartz grains compose up to 5% of the debris.

In addition to chlorite, quartz, and rutile, spherules in S4 also contain apatite (up to 50%), siderite (up to 50%), pyrite, and chalcopyrite. The rutile and chlorite are Cr rich.

Sedimentation. S4 is interbedded with coarse, conglomeratic, highly energetic fan-delta deposits. Although it contains some admixed terrigenous detritus, S4 consists largely of spherules, crushed spherules, irregular chlorite-rich grains, and fine chloritic matrix, all of which probably represent altered impact detritus. The sediments have been mixed and deposited by currents, but the amount of reworking has been insufficient to substantially dilute impact-produced materials with the surrounding much more abundant terrigenous sediment.

DISCUSSION

Identification and correlation of spherule beds

Although high-precision zircon dates, distinctive spherule types and compositions, and recognizable and traceable stratigraphic units have facilitated correlation of spherule beds among most BGB structural belts, uncertainties remain, particularly with respect to beds here correlated with S3. Many structural belts lack zircon dates, and in others available dates do not bracket the spherule beds present. There is a great deal of variability in the thickness, structuring, and composition of individual spherule beds from area to area, reflecting both the variable depositional environments into which the debris fell and the complex and variable postdepositional histories of the separate BGB structural blocks.

At its type locality at SAF-179, S3 shows abundant spherules containing Ni-rich spinels, a large Ir anomaly, and a wide variety of spherule types. These features also characterize beds identified as S3 in the Sheba Mine (SAF-381), the Princeton Tunnel of the Agnes Mine (SAF-379), the Florence and Devonian Mine (SAF-294), the Loop Road (SAF-295), and SAF-105 on the west limb of the Barite Syncline. Except for SAF-179 and 105, all of these localities are in the northern BGB and show S3 composed of nearly undiluted fall-deposited spherules that accumulated under quiet-water conditions with little or no postdepositional reworking. However, at the Mount Morgan Mine overlook (SAF-390), the spherule bed at the Fig Tree–Onverwacht contact, correlated with S3, shows only minor current working but lacks spinels and shows only a moderate Ir anomaly (12.6 ppb). The spherule bed at this locality lies within a few meters of one of the major frontal faults and may have been subject to severe metasomatism. Associated cherts are heavily bleached and altered. At SAF-388 and nearby localities in the Stolzburg Syncline (Fig. 7), the base of the Fig Tree Group is marked by a 1–2.5-m-thick unit of graded komatiite and chert-clast breccia and sandstone resting directly on spinifex-bearing komatiite flow units (Fig. 16). The upper sandy part of the bed contains sparse (<1%) spherules, none of which contains spinels. The bed also lacks an Ir anomaly, perhaps reflecting the small proportion of spherules and abundance of locally derived ripped-up debris. This bed is correlated with S3 based largely on its stratigraphic position beneath the Ulundi and Sheba Formations of the Fig Tree Group and above Onverwacht volcanic and cherty units, as at the Florence and Devonian Mine and Sheba Mine.

In the Barite Syncline (Fig. 3), a prominent and traceable spherule bed correlated with S3 lies 30–150 m above the base of the Fig Tree Group. On the east limb, the bed is ~140 m above black cherts of the Onverwacht Group and 150 m below Fig Tree strata dated at 3,225 Ma (Kröner *et al.*, 1991) and shows extensive reworking by tidal currents, a modest Ir anomaly (5.8 ppb), and few or no spinels. On the west limb (Fig. 14, SAF-105), there is an erosional unconformity at the base of the Fig Tree Group, and S3 is a 30–40-cm-thick bed 5–15 m above black cherts of the Onverwacht Group. Ir contents vary from as low as 4.5 ppb

1–2 km south of SAF-105 to 144.5 ppb at SAF-105, where there are abundant spinels. These sections illustrate the problems in correlating S3 within and among the many belts in which it occurs. As discussed below, a number of postdepositional processes may have locally enriched or depleted spinels and Ir in S3 and possibly S1 and S2. These may account for some of the observed variation in the composition and properties of individual beds. However, future studies may also suggest that in some areas beds here correlated with S3 may represent S2 or possibly other, as yet unrecognized spherule beds in the lower part of the Fig Tree Group.

Ir abundance

Spherule beds S3 and S4 display extreme Ir enrichment, locally up to 100% of chondritic levels, and Reimold *et al*. (2000) reported values up to 500% chondritic in S3 samples from the northern part of the BGB. This extreme Ir enrichment has led some investigators to question the impact origin of the BGB units and suggest that hydrothermal processes are responsible for high Ir levels in the spherule beds (Koeberl *et al.*, 1993; Koeberl and Reimold, 1995; Reimold *et al.*, 2000).

It now seems clear the BGB spherule beds represent debris produced by large meteorite impacts and that extreme Ir levels measured in individual samples do not reflect average bed values across the outcrop or within individual sections. Such locally high PGE contents have several possible origins: (1) Little is known about the condensation mechanics of impact-produced rock vapor clouds. Condensation within such clouds may involve element fractionation as a function of condensation temperature and local environment, and may over time yield spherules having a wide range of compositions. At any given moment or locality, the condensates may be greatly enriched in certain elements relative to the cloud as a whole. The falling spherules may thus change composition over time, and the resulting deposits may be extremely heterogeneous vertically and laterally. (2) At least some of the variation in Ir contents may reflect hydraulic fractionation of components of different sizes and densities during fall and, following deposition, by waves and currents. If some current-worked sections contain fewer Ni-rich spinels and low Ir values because of hydraulic fractionation of denser spinel-bearing spherules, other sections will show spinel enrichment, yielding locally high Ir values. S3 in Jay's chert, which contains up to 10% Ni-rich spinel-bearing spherules, may have been hydraulically enriched in such spherules and Ir, whereas S3 on the tidally influenced east limb of the Barite Syncline has apparently been depleted. S4, the basis of bolide modeling by Byerly and Lowe (1994) and Shukolyukov *et al*. (2000), consists of a single population of chloriterich spherules and spherule debris that would seem to offer little opportunity for similar hydraulic fractionation. Although showing evidence of some current activity, S4 has not been significantly diluted by terrigenous sediment, suggesting that it has not been significantly reworked or thickened by the addition of non–impact-produced material. The average Ir content of this layer may reflect the average Ir content of the impact-produced vapor cloud. The observed thickness probably represents a minimum estimate of the original thickness of S4 because of erosion of the bed top. However, because of the small extent of the outcrop of S4, the possibility that the thickness of the impact-produced debris has been increased by local reworking within the fan-delta system cannot be eliminated. (3) There has been a great deal of localized dissolution and stylolitization in sedimentary units in the BGB, particularly in areas of shearing and severe shortening. These processes tend to remove more mobile elements, leaving dark, dense stylolitic residues enriched in immobile components, probably including degraded spinels and Ir. The extreme Ir abundances recorded by Reimold *et al*. (2000) may represent immobile element residues of this type. (4) In areas of extreme hydrothermal alteration, shearing, and mineralization, it might be expected that there has been at least local redistribution of even largely immobile elements, such as Ir (Shukolyukov *et al.*, 2000). (5) Sampling of impact deposits and craters to date has been highly biased toward relatively young, Proterozoic and Phanerozoic features produced by relatively small impacts on continental crust. However, the Archean may have been dominated by much larger impacts on oceanic crust. Large impacts onto Archean mafic or ultramafic crust may have produced rock vapor clouds containing a higher proportion of bolide-sourced components than smaller Phanerozoic continental impacts. This explanation, however, cannot account for the extreme Ir heterogeneity exhibited by S2 and S3.

Origin of the spherule beds

As noted by Lowe and Byerly (1986), the presence of edge-centered inward radiating and lath-shaped and prismatic crystal pseudomorphs, dendritic spinels, pseudomorphs after barred olivine, and welded particles in BGB spherules indicates that they formed as liquid silicate droplets. There are only two common means by which abundant liquid silicate droplets form within surface environments: volcanic eruptions (mainly lava fountaining) and meteorite impacts. Several features of the distribution and composition of the spherule beds are inconsistent with a volcanic origin but consistent with formation through impacts: (1) S1, S2, and S3, where not removed by erosion or by postdepositional shearing, are of regional extent. S4 crops out over such a small area and the corresponding horizon in other sections is so poorly exposed that its extent has yet to be determined. S1, S2, and S3, however, are neither localized around possible eruption sites nor display regular proximal-to-distal facies, which might be expected if they originated as ballistic volcanic particles, such as lava-fountain droplets. (2) The spherules in S1, S2, and S3 accumulated as blankets that mantled surfaces within every depositional system into which they fell. In deep, quiet-water settings, they accumulated as fall-deposited layers without subsequent current working. In shallow water, spherules were generally reworked by waves and/or currents. These were clearly regional and possibly global layers, not the localized products of lava fountaining. (3) The presence of compositionally diverse spherules in all beds indicates that they did not form from single homogeneous magmas, like spherules formed as lava-fountain droplets. (4) The spherules are unlike any known volcanic particles of komatiitic, basaltic, or felsic composition in the BGB. Most exhibit internal textures, structures, and alteration compositions unlike those in ocelli, variolites, accretionary lapilli, devitrification spheroids, and other volcanic structures and particles within the BGB. (5) The spherule layers contain little or no clearly juvenile volcanic or pyroclastic materials, such as shards, vesicular grains, or phenocrysts. (6) The spherule beds are unique beds in the sections where they occur. Similar particles are absent outside of the beds except in rare instances where spherules or pieces of spherule beds have been eroded and deposited as part of younger sedimentary units or where spherules have been injected downward or upward through postdepositional soft-sediment mobilization (Fig. 14). (7) The spherules were originally smooth spheres, unlike all but rare particles produced by weathering and erosion, and locally compose 50–100% of beds S3 and S4 and 20–50% of S1 and S2. Their structuring, sphericity where undeformed, and abundance preclude an origin by simple erosion of volcanic rocks, as suggested by de Wit (1986) and Buick (1987).

A variety of geochemical evidence directly indicates that the BGB spherule beds formed as a result of large meteorite impacts: (1) Beds S3 and S4 are sites of major Ir enrichment; S1 and S2 host smaller but still significant Ir anomalies (Lowe *et al.*, 1989; Kyte *et al.*, 1992; Koeberl *et al.*, 1993; Reimold *et al.*, 2000). (2) The more immobile PGEs, Pt, Os, and Ir, display roughly chondritic ratios in S3 and S4, consistent with derivation from chondritic impactors (Kyte *et al.*, 1992). (3) Spinels in S3 display compositions unlike those of spinels in komatiites within the BGB and consistent with compositions expected in impact-related materials (Byerly and Lowe, 1994). (4) The Cr isotopic signatures in samples from beds S2, S3, and S4 indicate the presence of extraterrestrial Cr components and suggest carbonaceous chondrite projectiles (Shukolyukov *et al.*, 2000; Kyte *et al.*, 2003). (5) Komatiites have a Cr-to-Ir ratio that is similar to that of the Earth's primitive mantle, whereas the extreme Cr and Ir enrichments in S3 and S4 have a very different Cr-to-Ir ratio, similar to that in carbonaceous chondrites (Lowe *et al.*, 1989). Figure 19 displays the variation in Ir and Cr for the BGB spherule beds, chondritic meteorites, the primitive mantle, komatiitic volcanic rocks, and fine silicified komatiitic tuffs in the BGB, which also tend towards Ir and Cr enrichment. The trends for S3 and S4 are dispersed at lower Cr and Ir values, in part reflecting analytical uncertainties at sub-ppb levels but probably also reflecting dilution of one or both elements by non-impact sources. Even at the highly dispersed Cr/Ir ratio seen at Ir levels below 10 ppb, the discrimination between komatiites and spherule beds is complete, with both S1 and S2 beds showing compositions consistent with an impact origin. At these sub-10–ppb levels, however, intensively silicified komatiitic pyroclastic units also display the low Cr/Ir ratios found in impact beds. We have noted variable Cr loss in units where alteration is extreme, generally including loss of all

F19

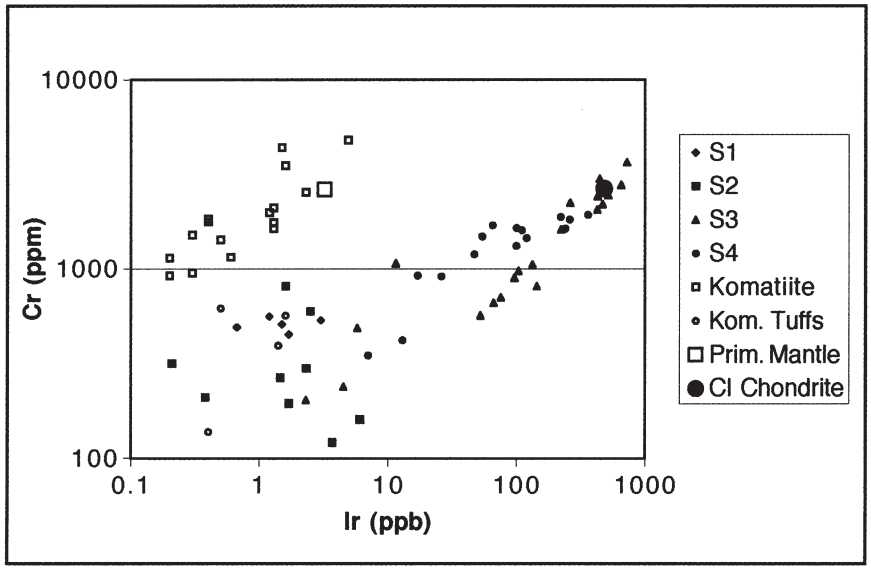

FIG. 19. Plot of Ir versus Cr in BGB spherule beds, BGB komatiitic flow rocks, silicified komatiitic pyroclastic units, primitive mantle, and CI chondrites. Except for some heavily silicified komatiitic pyroclastic units, the BGB spherule beds lie on a trend with CI chondrites and are distinct from the primitive mantle and komatiitic volcanic rocks.

divalent cations, especially Fe, Mg, and Ca. Apparently, extreme alteration also results in partial loss of Cr and displacement of Cr/Ir ratios into the field of impact materials.

Koeberl *et al*. (1993), Koeberl and Reimold (1995), and Reimold *et al*. (2000) have outlined a number of objections to the impact interpretation of the BGB spherule beds. Unfortunately, these authors confuse spherules and accretionary lapilli described by previous authors (Lowe and Knauth, 1977, 1978; Stanistreet *et al.*, 1981; Heinrichs, 1984). To our knowledge, none of the particles previously interpreted as accretionary lapilli has been reinterpreted to be impact-produced spherules, as claimed by Koeberl and Reimold (1995) and Reimold *et al.* (2000).

Arguments of Koeberl *et al*. (1993), Koeberl and Reimold (1995), and Reimold *et al*. (2000) against an impact origin of the BGB spherule beds include: (1) the high PGE and siderophile element abundances in the spherule beds; (2) the nonchondritic ratios of PGE elements and lack of correlation of siderophile elements (e.g., Ni and Ir); (3) the correlation between siderophile element abundances and the contents of chalcophile elements, such as S, As, and Sb; (4) the presence of local PGE enrichment in country rocks surrounding the spherule beds; (5) the compositions of Ni-rich spinels in BGB spherule samples, which they suggest are different from the compositions of spinels in known impact ejecta and meteorites; and (6) the absence of shocked minerals and metamorphism, which occur "even in 2-Ga-old impact structures, such as Vredefort and Sudbury."

The principal problem with the first four of these observations is that they derive mainly from samples collected in and around the Agnes and Sheba gold mines in the northern part of the BGB and fail to evaluate long-known processes of alteration and metasomatism that have affected rocks throughout the BGB (de Wit *et al.*, 1982; Smith and Erlank, 1982; Duchac and Hanor, 1987; Hanor and Duchac, 1990; de Wit and Hart, 1993; and many others). Rocks along the frontal part of the belt have in addition been widely subject to sulfide and Au mineralization, which could be expected to change ratios of more mobile (e.g., Ni, Au, Fe, S, Cu) to immobile (e.g., Ir, Cr) elements, and penetrative shearing and faulting, which might be expected to blur the spatial distribution of even immobile components, such as Ir. Observations that samples collected from such areas no longer preserve primary element ratios and distributions, especially at a small scale, should not be surprising.

The unusual Ir abundances have been discussed by Shukolyukov *et al*. (2000) and in this report above. As noted by Shukolyukov *et al*. (2000), Ir abundances as high as and higher than

those observed in the BGB spherule beds have been noted in the Cretaceous-Tertiary (K/T) boundary layer and meteorites, a fact overlooked by Koeberl *et al*. (1993) and Reimold *et al*. (2000). Extreme Ir levels cannot serve as an argument against an impact origin.

With regard to the unusual composition of spinels, all BGB spherule beds lie in close proximity, geographically and stratigraphically, to komatiitic lavas. Many of these volcanic rocks have been altered in a fashion similar to the spherule beds, including local loss of Fe and Mg and enrichment in Si and K. Yet in these altered komatiites the spinels retain igneous forms and compositions (Byerly, 1999). It seems unlikely that only the spinels within the spherule layers would undergo an unusual alteration to compositions not seen in any other terrestrial environment. Tredoux *et al*. (1989) reported Ni-rich spinels from a small area of nickel and PGE mineralization at Bon Accord in the northern BGB and proposed that they represent an unusual magmatic body derived from the core–mantle boundary. Earlier, de Waal (1978) had proposed that the Bon Accord body represents a meteorite. Koeberl and Reimold (1995) suggested that erosion of this deposit might explain the S3 spinels and PGE enrichments in the BGB spherule beds. As discussed by Glikson (2001), this scenario is not only highly unlikely geologically, but also the Ni-rich spinels of Bon Accord are quite different that those in S3. Bon Accord spinels are highly variable, with many displaying nearly end-member compositions for Ni, Co, and Ni-Co varieties, and contain relatively high Ti and no V (Tredoux *et al.*, 1989). The BGB impact spinels display a much simpler variation, nearly chondritic Ni/Co ratios, and low Ti and high V (Byerly and Lowe, 1994). The PGE patterns at Bon Accord also display extreme enrichments in more volatile PGEs, Rh, Pt, and Pd, relative to less volatile Os, Ir, and Ru, unlike PGE patterns in S3 (Byerly and Lowe, 1994).

Shocked minerals and shock metamorphic features have not been observed in the BGB spherule beds, but their presence in the Vredefort and Sudbury areas is irrelevant to the origin of the BGB spherule layers. Vredefort and Sudbury, and most preserved post-Archean impact sites, are on continental crust, yielding large amounts of coarse, relatively stable shocked minerals, such as quartz and zircons. The BGB impacts appear to have involved Archean oceanic crust, probably composed largely of komatiite and basalt (Byerly and Lowe, 1994), which would have yielded no shocked quartz or zircons. All ferromagnesian minerals and feldspars in the spherule beds have been completely altered. Few minerals remain that could be expected to show shock features, although some durable trace minerals that might show shock features or fine shock-produced minerals, such as diamonds or majorite, could be present.

Origin of the spherules

Studies of Phanerozoic impact deposits have shown that liquid silicate droplets can originate either as ballistic "splash" particles thrown out from impact sites or as condensates from clouds of rock vapor ejected above the atmosphere. Many BGB spherules were probably composed of glass and were similar to microtektites; others containing relict crystallites were similar to microkrystites (e.g., Glass and Burns, 1988; Glass *et al.*, 1988; Glass and Koeberl, 1999; Smit, 1999). Differences in the abundance and degree of preservation of crystalline textures in S2 and S3 among different sections of the same bed suggest that pervasive postdepositional diagenesis and metasomatism may have obliterated many primary crystalline textures.

Lowe and Byerly (1987), Lowe *et al*. (1989), Kyte *et al*. (1992), and Byerly and Lowe (1994) concluded that the BGB spherules formed by condensation of global clouds of impact-generated rock vapor. Estimates of bolide size by Sleep *et al*. (1989), Melosh and Vickery (1991), and Shukolyukov *et al*. (2000) and of crater size by Glikson (2001) were based on similar assumptions. This conclusion is suggested by a combination of features: (1) All four beds appear to represent distal impact deposits. S3, where not reworked by currents, consists of nearly undiluted spherules and spherule fragments. Most of S4 is also composed largely of spherules or spherule debris. No large ballistic clasts have been identified in the BGB spherule beds, and only current-deposited S1 includes irregular particles similar to the spherules in composition and size that might represent ballistic debris. Younger layers made up of ballistic spherules also typically contain a significant proportion of other, nonspherical ejecta (Glass and Koeberl, 1999; Smit, 1999). It is difficult to picture how the 30–35 cm of relatively undiluted spherules in fall-deposited sec-

tions of S3 could accumulate as ballistic particles without abundant associated angular ballistic debris. (2) The formation of large rock vapor clouds and production of global condensate layers is associated with impacts of larger bolides. The K/T bolide was ~10 km in diameter and produced a global spherule-rich condensate or "fireball" layer (Hildebrand and Boynton, 1990; Pope, 2002) ~3 mm thick (Smit, 1999). S3 is 25–35 cm thick in its several fall-deposited sections, and average sections of S1 and S2 would yield undiluted spherule beds at least 2–5 cm thick. These extraordinarily thick distal spherule beds suggest enormous bolides, considerably larger than the K/T bolide, as does a variety of other evidence (Sleep *et al.*, 1989; Melosh and Vickery, 1991; Byerly and Lowe, 1994; Shukolyukov *et al.*, 2000). Such large bolides could be expected to produce large rock vapor clouds, much of which would have been ejected above the atmosphere, consistent with the formation of abundant condensate spherules. (3) The spherules in S3 contain Ni-rich spinels having compositions like those in chondrites and unlike those in probable targets rocks (Byerly and Lowe, 1994), whereas loose, detrital spinels in the same current-worked beds are compositionally like those in komatiites. Splash-produced spherules typically contain a high proportion of target rock. However, spinel compositions, PGE abundances in S4 (Kyte *et al.*, 1992), and model bolide/target rock mixtures for S3 (Byerly and Lowe, 1994) indicate high proportions of bolide in these layers. (4) All beds include common spherules showing pseudomorphs after primary crystallites (Figs. 11F and G and 15E, F, and H). Younger microkrystites are characteristic of distal deposits (Glass and Koeberl, 1999) formed by vapor condensation (Smit, 1999). (5) BGB spherules include rare agglutinated forms (Fig. 11C) but few teardrop, button-shaped, or other nonspherical forms common to younger splash-produced microtektite layers (Glass and Koeberl, 1999; Smit, 1999). (6) Vesicular spherules are common in younger microtektite layers (Smit, 1999) but are not known in the BGB spherule beds. Collectively, these features seem most consistent with spherules formed through vapor condensation and deposited distally, far from the craters and near-crater sites of impact breccia and fringing ballistic ejecta deposition.

However, many spherules in the BGB beds may have been composed largely of glasses, which are most common in ballistic microtektites (Glass and Koeberl, 1999; Smit, 1999), and a few have shapes that could reflect atmospheric drag on liquid droplets (e.g., Fig. 11D and E). Although it seems likely that the great bulk of BGB spherules formed as condensates, it is possible that some represent chilled ballistic splash grains ejected above the atmosphere along with the rock vapor clouds.

Present spherule compositions in beds S1, S2, and S3 range from nearly pure silica to nearly pure sericite or chlorite. These compositions are the products of long and complex alteration histories that may have included early diagenetic clay- and feldspar-bearing mineral assemblages similar to those in spherules from the K/T boundary (Montanari *et al.*, 1983; Bohor and Glass, 1995; Smit, 1999). It seems likely that the present range of BGB-spherule mineralogy reflects a range of original compositions from virtually alumina free to highly aluminous glasses. BGB microkrystites included spinel-, olivine-, and possibly pyroxene-bearing varieties similar to those in the K/T condensate layer (Smit, 1999). Their presence mixed within individual beds and vertical changes in spherule size and composition in fall-deposited sections of S3 (Fig. 13) probably reflect differing environments within the vapor cloud, complex condensation histories, and hydraulic fractionation of spherules during fall.

Byerly and Lowe (1994) estimated the probable target and bolide mixture using the average immobile-element composition of S3: 12.5% Al_2O_3, 0.75% TiO_2, 1,000 ppm Cr, 40 ppm Zr, and 78 ppb Ir. The model results suggest that the spherules represent a mixture of >70% basalt, ~15% komatiite, ~15% carbonaceous chondrite, and <2% dacite. S4 spherules lack quench textures and spinels and were probably composed of glass. Compositional modeling of this layer requires a similar mix of target and bolide lithologies, perhaps containing up to 25% bolide (Byerly and Lowe, 1994).

Sedimentation of the spherule beds

S1, S2, and S3 were deposited over wide areas under what are inferred to have been marine conditions. Both S1 and S2 were deposited mainly in quiet, low-energy, subaqueous environments, as indicated by the dominance of fine black carbonaceous chert, black-and-white banded chert, laminated ferruginous chert, and fine silicified tuffs in underlying and overlying rocks. Small-

scale cross-lamination in some tuffaceous layers indicates sporadic weak currents, but lack of large cross-stratification, coarse clastic units, and scour features outside of the spherule beds indicates that the overall settings were quiet, low-energy, and possibly moderately to deep water. Within these settings, S1 and S2 mark short-lived, high-energy events that resulted in widespread erosion of underlying sediments and volcanic rocks. Erosion produced abundant, mainly locally derived clastic material that diluted the impact-produced particles. The resulting beds exhibit clastic textures, show wave and/or current structures, and contain low to moderate proportions of spherules. The beds are commonly graded, with coarse rip-up clasts in the lower parts and sand-sized material above, indicating that the depositing waves and/or currents behaved as surges, beginning abruptly and waning gradually over time. These high-energy events within otherwise low-energy depositional environments are interpreted to have been tsunamis generated by the impacts. Most rip-up clasts have compositions indicating derivation from underlying rocks.

S1 locally and S2 throughout most of its known outcrop are compound beds, including two distinct graded current-deposited units (Figs. 4 and 9). In SAF-272, a bed of gray chert 25 cm thick, representing silicified fine sand, silt, and organic matter, separates a lower graded unit of coarse spherule-bearing breccia and sandstone and an upper graded unit of spherule-bearing sandstone (Fig. 9). This black chert layer marks a short-lived quiescent interval during which suspended fine sediment settled out of the water column. As at SAF-374 (Fig. 9), the lower graded unit is typically coarser than the upper unit. The presence of paired graded beds indicates that deposition of S1 and S2 involved at least two distinct, energetic, surge-like current and/or wave events separated by short intervals of reduced wave or current activity. These events are thought to reflect the passage of two or more distinct tsunami wave sets, possibly resulting from modulated wave trains that wax and wane during passage (Hassler *et al.*, 2000), reflection off of surrounding land areas, or radiation back from a point of convergence at the antipode to the impact site.

S3 was deposited across a wide range of environments from coastal fan delta and shallow, current-swept subtidal settings in southern and central areas to quiet, deeper-water sites along the northern margin of the BGB. In most areas, S3 debris was worked by tsunamis during and immediately following deposition. In deeper, quieter environments, the tsunamis had less effect on the sea floor, and S3 consists largely of normally graded fall-deposited spherules and spherule fragments (Fig. 13).

Impact-generated tsunamis are also thought to have influenced deposition of Late Archean and Early Proterozoic spherule beds (Hassler *et al.*, 2000; Hassler and Simonson, 2001; Simonson and Hassler, 2002). They also swept and eroded marginal marine and coastal settings around the Gulf of Mexico as a result of the K/T impact (Bourgeois *et al.*, 1988; Habib *et al.*, 1996; Smit *et al.*, 1996).

Bolide and crater size estimates

Sleep *et al*. (1989) first suggested the scale of the BGB impacts. Using gross thickness of S3 in fall-deposited sections and assuming that the bed is a worldwide layer, they estimated an energy release consistent with a bolide 30 km in diameter. Based on the approach of OnKeefe and Ahrens (1982), Lowe *et al*. (1989) used the maximum diameter of spherules condensed from a impact rock vapor cloud, ~3 mm in S3, to suggest that bolide sizes for the BGB impacts were in the range of 20–50 km. Melosh and Vickery (1991) used several spherule-size models to suggest that these Archean impact bolides could have had diameters in excess of 100 km. Kyte *et al*. (1992) calculated an Ir fluence for S4 consistent with a bolide >20 km in diameter, and, based on the Ir fluence for S3, Byerly and Lowe (1994) suggested a bolide ~30 km in diameter. Byerly and Lowe (1994) also did a detailed size analysis for S3 and concluded that using the average size for the smallest population of spherules, those with Ni-rich spinel, which have an average diameter of 0.85 mm, yields a bolide size of 24 km. Shukolyukov *et al*. (2000) found the extraterrestrial chromium in S4 required a chondritic fluence about one-third greater than that previously estimated from Ir. In summary, various parameters have been used to estimate the size of these Archean impactors, including bed thickness, spherule size, Ir fluence, and extraterrestrial Cr fluence. Most yield comparable estimates of 20–50 km diameter for the bolides. It needs to be stressed, however, that bolide-size estimates based on Ir and Cr fluence assume that the layers were deposited globally at thicknesses comparable those in the least current-

worked sections. At present, there is no direct evidence that any layers except S1 were or were not deposited globally.

Glikson (2001) scaled bolide diameters by a factor of 20 to suggest that the craters produced were in the range of 400–1,000 km in diameter. This range compares well with the sizes of impact basins on the Moon, which formed 300–500 million years earlier. Bailly, Schrodinger, and Medeleev are all ~300 km in diameter, while the largest basins, Orientale, Imbrium, and Chisium, are ~1,000 km in diameter. Total energy released globally (e.g., Sleep *et al.*, 1989), and even locally as thick accumulations of hot impact spherules fell to Earth, would have been very significant. The formation of three or four craters on Earth, each 400–1,000 km diameter, would have also had profound effects on global geological and biological processes.

Implications for early life

Potential deleterious effects of large impacts on early organisms and biological communities have been extensively discussed (e.g., Maher and Stevenson, 1988; Oberbeck and Fogleman, 1989; Sleep *et al.*, 1989; Zahnle and Sleep, 1997; Sleep and Zahnle, 1998). Large impacts, like that responsible for deposition of S3 and possibly the other BGB spherule beds, would have evaporated a substantial thickness of ocean water, leaving behind a thick surface layer of "boiled brine" (Sleep and Zahnle, 1998); enveloped the Earth in a blanket of hot dust and steam; blanketed the global land surface and sea floor with thick layers of ejecta; and otherwise severely disrupted surface ecosystems. Some of these effects would have been mitigated if early Archean surface temperatures were already hot, perhaps as high as 70 ± 15°C (Knauth and Lowe, 2003), and the early oceans highly saline (Knauth, 1998) so that early biological communities were already composed largely or exclusively of thermophiles and halophiles.

Extreme effects, including sterilization of the Earth, would probably have obtained only during very early accretion (Ryder, 2002), although the results of this study suggest that large impacts may have extended into younger parts of geologic time than previously suspected. Later large, but not sterilizing, impacts may have actually stimulated the biological community. Klein and Beukes (1989), Lowe (1994), and many others have suggested that the Archean oceans were strongly stratified, with a deep anoxic, Fe-rich bottom layer and a thin, wind-mixed, Fe-poor upper layer. Without adequate mixing and in the absence of continental runoff, the upper layer of an Archean stratified ocean may have been depleted in nutrients and was perhaps a vast biological desert (Lowe, 1994). Large impacts like those discussed here and the resulting tsunamis would have provided a mixing mechanism that would have stirred the oceans and brought nutrient-rich deep waters to the surface. If frequent, such impacts may have provided an important mechanism for deep- and shallow-water mixing in the Archean oceans and for nutrient enrichment of waters within the photic zone.

Tectonic implications

S1 occurs within a basaltic to komatiitic volcanic section, and there is little or no evidence of any changes in the overall volcanic or tectonic regime following deposition. S4 is so local in known outcrop that it is not possible to evaluate possible regional or global effects of the impact.

Along the northern margin of the BGB, in both the Florence and Devonian Mine and Princeton Tunnel, altered komatiitic volcanic rocks below S3 are cut by black chert dikes containing spherules (Fig. 14). These dikes extend downward from 5 to >50 m, crosscutting primary and early alteration features in the volcanic rocks (Lowe *et al.*, 1999, their Fig. 3). Similar dikes occur below S3 in the Barite Syncline (Fig. 14). Spherules are present in the dikes as individual loose grains, indicating that S3 was unlithified when injection occurred. At the Florence and Devonian Mine, S3 is overlain within a few meters by shale containing thin jasper layers and then a thick Fig Tree graywacke sequence. No debris from these overlying units is present in the chert dikes, indicating that diking occurred penecontemporaneously with deposition of S3 and before clastic sedimentation began. It seems possible that fracturing of the komatiitic flow sequence may have been a consequence of crustal stresses associated with impacting and that the soft black-chert precursor sediments and accumulating spherules exploited these fractures to form the dikes. Similar deformations, including faulting and the capture of spherule-bearing sediments in impact-generated fault-bounded depressions, have been reported >1,000 km from the K/T impact site (Olsson *et al.*, 1996; Smit *et al.*, 1996).

S2 and S3 mark profound local and possibly regional changes in tectonic regime. In the southern BGB, S2 marks the change from basaltic and komatiitic volcanic rocks and cherts of the Onverwacht Group to ferruginous sediments, felsic ash, and clastic units of the lower Fig Tree Group at ~3,260 Ma. In the northern BGB, S2 has not been identified, but the corresponding horizon probably lies somewhere in the upper part of the Mendon and Weltevreden Formations of the Onverwacht Group. In this area, S3 marks the transition from Onverwacht komatiites and black cherts to Fig Tree ferruginous sediments, shale, and sandstones at 3,243 ± 4 Ma (Kröner *et al.*, 1991). These impacts marked the end of a 300-million-year-long interval of predominantly basaltic and komatiitic volcanism and chemical and biological sedimentation under anorogenic conditions (Onverwacht Group) and the beginning of an interval of uplift, deformation, and clastic sedimentation (Fig Tree Group). The basal Fig Tree rocks represent the first major terrigenous clastic units in BGB evolution.

Two such abrupt changes, closely spaced in time, each marked by a major impact layer, seem more than coincidental. Major impacts at 3,260–3,240 Ma may have triggered regional if not global reorganization of tectonic systems, crustal deformation that led to uplift associated with Fig Tree and Moodies deposition, terrain amalgamation, and, ultimately, the formation of the Kaapvaal Craton at ~3.2–3.1 Ga. Glikson (1999, 2001) also discussed in some detail the possible consequences of very large impacts for terrestrial tectonism.

Impact history of the early Earth

The four spherule layers in the BGB represent distal deposits of four major impacts over an interval of ~225 million years. Based on the net thickness of spherules and locally enormous Ir enrichment, these impacts were larger than any known from the entire Phanerozoic, an interval of ~540 million years. To date, we have identified at least two and possibly three other spherule beds in the BGB, all younger than S1. The uppermost is ~3,225 Ma in age and marks the contact of the Sheba and Belvue Road Formations of the Fig Tree Group in the Stolzburg Syncline (Fig. 3). It was labeled S3? by Byerly and Lowe (1994, their Fig. 2, northern facies). Although these beds have not been studied in detail and are not described here, they may offer additional evidence of large impacts on the pre-3.0 Ga Archean Earth. The clustering of spherule beds in the Fig Tree Group, 3,260–3,225 Ma, is consistent with the inference by Glikson (2001) based in part on data of Culler *et al*. (2000) that the lunar record shows a spike in impacts at ~3.2 Ga. However, it should also be noted that deposition of the Fig Tree Group was accompanied by the wide development of quiet- and commonly deep-water environments favorable to the accumulation and long-term preservation of fall-deposited impact materials. The preceding 300 million years of Onverwacht time was dominated by volcanism: Sediments constitute a minor part of the geologic record of this interval, although the time they represent may be significantly greater than their relative thickness. Deposition of the Moodies Group was dominated by sedimentation in energetic alluvial and shallow marine environments. Spherules falling into these systems would have been rapidly reworked and mixed and diluted with terrigenous sediments. The distribution of spherule beds in the BGB corresponds to the distribution of depositional settings favorable for their accumulation and preservation.

Hassler and Simonson (2001) and Simonson and Hassler (2002) have identified five thick impact-generated spherule layers 2.64–2.5 Ga in Western Australia and South Africa. These units also occur in rocks deposited mainly under quiet-water conditions, not unlike those that characterized deposition of much of the Fig Tree Group. Rocks representing the intervening 500 million years, from 3.2 to 2.7 Ga, are principally volcanic units and energetic alluvial, fan-delta, shallow-water, and turbiditic deep-water clastic units. It may be that the present distribution of impact-generated beds within Archean rocks reflects the distribution of depositional conditions favorable to their accumulation and preservation rather than the temporal variability in the impact rate. Ryder (2002) suggested that the terrestrial impact rate declined from ~100 times to about twice the present-day rate between ~3.8 to 3.0 Ga, averaging ~15 times over this interval. The numbers of beds representing large-body impacts 3.26–3.22 Ga and 2.65–2.5 Ga suggest that actual impact rates during these intervals were considerably higher that this estimate. It is possible that impact "storms" during Archean were concentrated in a few narrow temporal windows, one ~3.3–3.2 Ga and another at 2.65–2.5 Ga, which just happened

to coincide with the deposition of a series of major sedimentary units that would favor preservation of fall-deposited impact-generated materials. Alternatively, the terrestrial flux of large impactors may have been significantly higher over much or all of the Archean than is suggested by the lunar impact record.

ACKNOWLEDGMENTS

The authors would like to acknowledge support from grants NCC2-721 and NAG5-9842 from the Exobiology Program to D.R.L.; NSF grant EAR-9909684 to G.R.B.; NASA grant NAG5-9411 to F.T.K.; and NASA grant NAG5-8172 from the Cosmochemistry Division to A.S. We are also grateful to the Avgold Division of the Anglo Vaal Mining Corporation, especially Hilton Philpot and Roelf le Roux, and the Anglo American Mining Corporation, South Africa, for access to properties, samples, and logistical support throughout this study. We would like to thank the Mpumalanga Parks Board, and especially Marc Stalmans, Louis Loock, and Johan Eksteen, for allowing us access to the Songimvelo Game Reserve. We are grateful to Bruce Simonson and an anonymous reviewer for offering many constructive suggestions for improvement of the manuscript.

ABBREVIATIONS

BGB, Barberton Greenstone Belt; K/T, Cretaceous-Tertiary; PGE, platinum group element.

REFERENCES

Bohor, B.F. and Glass, B.P. (1995) Origin and diagenesis of K/T impact spherules—from Haiti to Wyoming and beyond. *Meteoritics* 30, 182–198.

Bourgeois, J., Hansen, T.A., Wiberg, P.L., and Kauffman, E.G. (1988) A tsunami deposit at the Cretaceous-Tertiary boundary in Texas. *Science* 241, 567–570.

Buick, R. (1987) Comment on "Early Archean silicate spherules of probable impact origin, South Africa and Western Australia." *Geology* 15, 180–181.

Byerly, G.R. (1999) Komatiites of the Mendon Formation: late-stage ultramafic volcanism in the Barberton Greenstone Belt. In *Special Paper 329: Geologic Evolution of the Barberton Greenstone Belt, South Africa*, edited by D.R. Lowe and G.R. Byerly, Geological Society of America, Boulder, CO, pp. 189–212.

Byerly, G.R. and Lowe, D.R. (1994) Spinel from Archean impact spherules. *Geochim. Cosmochim. Acta* 58, 3469–3486.

Byerly, G.R., Kröner, A., Lowe, D.R., Todt, W., and Walsh, M.W. (1996) Prolonged magmatism and time constraints for sediment deposition in the early Archean Barberton Greenstone Belt: evidence from the upper Onverwacht and Fig Tree Groups. *Precambrian Res.* 78, 125–138.

Byerly, G.R., Lowe, D.R., Wooden, J.L., and Xie, X. (2002) An Archean impact layer from the Pilbara and Kaapvaal Cratons. *Science* 297, 1325–1327.

Chyba, C.F. and Sagan, C. (1997) Comets as a source of prebiotic organic molecules for the early Earth. In *Comets and the Origin and Evolution of Life*, edited by P.J. Thomas, C.F. Chyba, and C.P. McKay, Springer, New York, pp. 147–174.

Cloete, M. (1999) *Geological Society of South Africa Memoir 84: Aspects of Volcanism and Metamorphism of the Onverwacht Group Lavas in the Southwestern Portion of the Barberton Greenstone Belt*, Geological Society of South Africa, Johannesburg.

Condie, K.C., Macke, J.E., and Reimer, T.O. (1970) Petrology and geochemistry of early Precambrian graywackes from the Fig Tree Group, South Africa. *GSA Bull.* 81, 2759–2776.

Conley, C.D. (1977) Origin of distorted ooliths and pisoliths. *J. Sediment. Petrol.* 47, 554–564.

Culler, T.S., Becker, T.A., Muller, R.A., and Renne, P.A. (2000) Lunar impact history from $^{40}Ar/^{39}Ar$ dating of glass spherules. *Science* 287, 1785–1788.

de Waal, S.A. (1978) The nickel deposit at Bon Accord, Barberton, South Africa—a proposed paleometeorite. In *Special Publication 4: Mineralization in Metamorphic Terranes*, edited by W.J. Verwoerd, Geological Society of South Africa, Johannesburg, pp. 87–98.

de Wit, M.J. (1986) A possible origin for chondrule-like particles in the 3.6–3.3 Ga Barberton greenstone belt, South Africa. In *Lunar and Planetary Science Conference 17*, Lunar and Planetary Institute, Houston, pp. 182–183.

de Wit, M.J. and Hart, R. (1993) Earthns earliest continental lithosphere, hydrothermal flux and crustal recycling. *Lithos* 30, 309–335.

de Wit, M.J., Hart, R., Martin, A., and Abbott, P. (1982) Archean abiogenic and probable biogenic structures associated with mineralized hydrothermal vent systems and regional metasomatism, with implications for greenstone belt studies. *Econ. Geol.* 77, 1783–1801.

Delsemme, A. (1997) The origin of the atmosphere and of the oceans. In *Comets and the Origin and Evolution of Life*, edited by P.J. Thomas, C.F. Chyba, and C.P. McKay, Springer, New York, pp. 29–68.

Duchac, K.C. and Hanor, J.S. (1987) Origin and timing of the metasomatic silicification of an early Archean komatiite sequence, Barberton Mountain Land, South Africa. *Precambrian Res.* 37, 125–146.

French, B.M. (1987) Comment on "Early Archean silicate spherules of probable impact origin, South Africa and Western Australia." *Geology* 15, 178–179.

French, B.M. (1998) *LPI Contribution 954: Traces of Catastrophe: A Handbook of Shock-Metamorphic Effects in Terrestrial Meteorite Impact Structures*, Lunar and Planetary Institute, Houston.

Glass, B.P. and Burns, C.A. (1988) Microkrystites: a new term for impact-produced glassy spherules containing primary crystallites. In *Lunar and Planetary Science Conference 18*, edited by G. Ryder, Pergamon, New York, pp. 455–458.

Glass, B.P. and Koeberl, C. (1999) Ocean Drilling Project Hole 689B spherules and upper Eocene microtektite and clinopyroxene-bearing spherule strewn fields. *Meteoritics Planet. Sci*. 34, 197–208.

Glass, B.P., Burns, C.A., Crosbie, J.R., and DuBois, D.L. (1985) Late Eocene North American microtektites and clinopyroxene-bearing spherules. *J. Geophys. Res*. 90, D175–D196.

Glikson, A.Y. (1999) Oceanic mega-impacts and crustal evolution. *Geology* 27, 387–390.

Glikson, A.Y. (2001) The astronomical connection of terrestrial evolution: crustal effects of post-3.8 Ga mega-impact clusters and evidence for major 3.2+/−0.1 Ga bombardment of the Earth-Moon system. *Geodynamics* 32, 205–229.

Habib, D., Olsson, R.K., Liu, C., and Moshkovitz, S. (1996) High-resolution biostratigraphy of sea-level low, biotic extinction, and chaotic sedimentation at the Cretaceous-Tertiary boundary in Alabama, north of Chicxulub crater. In *Special Paper 307: The Cretaceous-Tertiary Event and Other Catastrophes in Earth History*, edited by G. Ryder, D. Fastovsky, and S. Gartner, Geological Society of America, Boulder, CO, pp. 243–252.

Hanor, J.S. and Duchac, K. (1990) Isovolumetric silicification of Early Archean komatiites: geochemical mass balances and constraints on origin. *J. Geol*. 98, 863–877.

Hassler, S.W. and Simonson, B.M. (2001) The sedimentary record of extraterrestrial impacts in deep shelf environments—evidence from the early Precambrian. *J. Geol*. 109, 1–19.

Hassler, S.W., Robey, H.F., and Simonson, B.M. (2000) Bedforms produced by impact-generated tsunami, ~2.6 Ga Hamersley Basin, Western Australia. *Sediment. Geol*. 135, 283–294.

Heinrichs, T.K. (1984) The Umsoli Chert, turbidite testament for a major phreatoplinian event at the Onverwacht/Fig Tree transition (Swaziland Supergroup, Archaean, South Africa). *Precambrian Res*. 24, 237–283.

Heinrichs, T.K. and Reimer, T.O. (1977) A sedimentary barite deposit from the Archean Fig Tree Group of the Barberton Mountain Land (South Africa). *Econ. Geol*. 72, 1426–1441.

Hildebrand, AR. and Boynton, W.V. (1990) Proximal Cretaceous-Tertiary boundary impact deposits in the Caribbean. *Science* 248, 843–847.

Klein, C. and Beukes, N.J. (1989) Geochemistry and sedimentology of a facies transition from limestone to iron-formation deposition in the early Proterozoic Transvaal Supergroup, South Africa. *Econ. Geol*. 84, 1733–1774.

Knauth, L.P. (1998) Salinity history of the Earth's early ocean. *Nature* 395, 554–555.

Knauth, L.P. and Lowe, D.R. (2003) High Archean climatic temperature inferred from oxygen isotope geochemistry of cherts in the 3.5 Ga Swaziland Supergroup, South Africa. *GSA Bull*. (in press).

Koeberl, C. and Reimold, W.U. (1995) Early Archaean spherule beds in the Barberton Mountain Land, South Africa: no evidence for impact origin. *Precambrian Res*. 74, 1–33.

Koeberl, C., Reimold, W.U., and Boer, R.H. (1993) Geochemistry and mineralogy of Early Archean spherule beds, Barberton Mountain Land, South Africa: evidence for origin by impact doubtful. *Earth Planet. Sci. Lett*. 119, 441–452.

Kröner, A., Byerly, G.R., and Lowe, D.R. (1991) Chronology of early Archaean granite-greenstone evolution in the Barberton Mountain Land, South Africa, based on precise dating by single zircon evaporation. *Earth Planet. Sci. Lett*. 103, 41–54.

Kyte, F.T., Zhou, L., and Lowe, D.R. (1992) Noble metal abundances in an Early Archean impact deposit. *Geochim. Cosmochim. Acta* 56, 1365–1372.

Kyte, F.T., Shukolyukov, A., Lugmair, G.W., Lowe, D.R., and Byerly, G.R. (2003) Early Archean spherule beds: chromium isotopes confirm origin through multiple impacts of projectiles of carbonaceous chondrite type. *Geology* (in press).

Lowe, D.R. (1994) Early environments: constraints and opportunities for early evolution. In *Nobel Symposium No. 84: Early Life on Earth*, edited by S. Bengston, Columbia University Press, New York, pp. 24–35.

Lowe, D.R. (1999) Petrology and sedimentology of cherts and related silicified sedimentary rocks in the Swaziland Supergroup. In *Special Paper 329: Geologic Evolution of the Barberton Greenstone Belt, South Africa*, edited by D.R. Lowe and G.R. Byerly, Geological Society of America, Boulder, CO, pp. 83–114.

Lowe, D.R. and Byerly, G.R. (1986) Early Archean silicate spherules of probable impact origin, South Africa and Western Australia. *Geology* 14, 83–86.

Lowe, D.R. and Byerly, G.R. (1987) Reply to comments on "Early Archean silicate spherules of probable impact origin, South Africa and Western Australia." *Geology* 15, 179–180, 181–182.

Lowe, D.R. and Byerly, G.R. (1999) Stratigraphy of the west-central part of the Barberton Greenstone Belt, South Africa. In *Special Paper 329: Geologic Evolution of the Barberton Greenstone Belt, South Africa*, edited by D.R. Lowe and G.R. Byerly, Geological Society of America, Boulder, CO, pp. 1–36.

Lowe, D.R. and Knauth, L.P. (1977) Sedimentology of the Onverwacht Group (3.4 billion years), Transvaal, South Africa, and its bearing on the characteristics and evolution of the early earth. *J. Geol*. 85, 699–723.

Lowe, D.R. and Knauth, L.P. (1978) The oldest marine carbonate ooids reinterpreted as volcanic accretionary lapilli, Onverwacht Group, South Africa. *J. Sediment. Petrol*. 48, 709–722.

Lowe, D.R. and Nocita, B.W. (1999) Foreland basin sedimentation in the Mapepe Formation, southern-facies Fig Tree Group. In *Special Paper 329: Geologic Evolution of the Barberton Greenstone Belt, South Africa*, edited by D.R. Lowe and G.R. Byerly, Geological Society of America, Boulder, CO, pp. 233–258.

Lowe, D.R., Byerly, G.R., Asaro, F., and Kyte, F.T. (1989) Geological and geochemical record of 3400-million-year-old terrestrial meteorite impacts. *Science* 245, 959–962.

Lowe, D.R., Byerly, G.R., and Heubeck, C. (1999) Structural divisions and development of the west-central part of the Barberton Greenstone Belt. In *Special Paper 329: Geologic Evolution of the Barberton Greenstone Belt, South Africa*, edited by D.R. Lowe and G.R. Byerly, Geological Society of America, Boulder, CO, pp. 37–82.

Lugmair, G.W. and Shukolyukov, A. (1998) Early solar system timescales according to ^{53}Mn-^{53}Cr systematics. *Geochim. Cosmochim Acta* 62, 2863–2886.

Maher, K.A. and Stevenson, D.J. (1988) Impact frustration of the origin of life. *Nature* 331, 612–614.

Melosh, H.J. and Vickery, A.M. (1991) Melt droplet formation in energetic impact events. *Nature* 350, 494–497.

Montanari, A., Hay, R.L., Alvarez, W., Asaro, F., Michel, H.V., Alvarez, L.W., and Smit, J. (1983) Spheroids at the Cretaceous-Tertiary boundary are altered impact droplets of basaltic composition. *Geology* 11, 668–671.

Oberbeck, V.R. and Fogleman, G. (1989) Impacts and the origin of life. *Nature* 339, 434.

O'Keefe, J.D. and Ahrens, T.J. (1982) The interaction of the Cretaceous/Tertiary extinction bolide with the atmosphere, ocean, and solid Earth. In *Special Paper 190: Geological Implications of Impacts of Large Asteroids and Comets on the Earth*, edited by L.T. Silver and P.H. Schultz, Geological Society of America, Boulder, CO, pp. 103–120.

Olsson, R.K., Liu, C., and van Fossen, M. (1996) The Cretaceous-Tertiary catastrophic event at Millers Ferry, Alabama. In *Special Paper 307: The Cretaceous-Tertiary Event and Other Catastrophes in Earth History*, edited by G. Ryder, D. Fastovsky, and S. Gartner, Geological Society of America, Boulder, CO, pp. 263–278.

Paris, I., Stanistreet, I.G., and Hughes, M.J. (1985) Cherts of the Barberton Greenstone Belt interpreted as products of submarine exhalative activity. *J. Geol*. 93, 111–129.

Pope, K.O. (2002) Impact dust not the cause of the Cretaceous-Tertiary mass extinction. *Geology* 30, 99–102.

Reimer, T.O. (1983) Pseudo-oolites in rocks of the Ulundi Formation, lower part of the Archaean Fig Tree Group (South Africa). *Precambrian Res*. 20, 375–390.

Reimold, W.U., Koeberl, C., Johnson, S., and McDonald, I. (2000) Early Archean spherule beds in the Barberton Mountain Land, South Africa: impact or terrestrial origin. In *Impacts and the Early Earth*, edited by I. Gilmour and C. Koeberl, Springer-Verlag, Berlin, pp. 117–180.

Ryder, G. (2002) Bombardment of the Hadean Earth: wholesome or deleterious? In *Impacts and the Origin, Evolution, and Extinction of Life: A Rubey Colloquium*, University of California, Los Angeles, pp. 49–52. Available at: http://www.ess.ucla.edu/rubey/index.html.

Ryder, G., Koeberl, C., and Mojzsis, S.J. (2000) Heavy bombardment of the Earth at ~3.85 Ga: the search for petrographic and geochemical evidence. In *Origin of Earth and Moon*, edited by R.M. Canup and K. Righter, University of Arizona Press, Tucson, pp. 475–492.

Schoenberg, R., Kamber, B.S., Collerson, K.D., and Moorbath, S. (2002) Tungsten isotope evidence from ≈3.8-Gyr metamorphosed sediments for early meteorite bombardment of the Earth. *Nature* 418, 403–405.

Shukolyukov, A., Kyte, F.T., Lugmair, G.W., Lowe, D.R., and Byerly, G.R. (2000) The oldest impact deposits on Earth—first confirmation of an extraterrestrial component. In *Impacts and the Early Earth*, edited by I. Gilmour and C. Koeberl, Springer-Verlag, Berlin, pp. 99–116.

Simonson, B.M. and Hassler, S.W. (2002) Spherule event horizons: the other (and better?) record of impacts in early Earth history. In *Impacts and the Origin, Evolution, and Extinction of Life: A Rubey Colloquium*, University of California, Los Angeles, CA, pp. 53–56. Available at: http://www/ess/ucla.edu/rubey/index.html.

Sleep, N.H. and Zahnle, K. (1998) Refugia from asteroid impacts on early Mars and the early Earth. *J. Geophys. Res*. 103, 28529–28544.

Sleep, N.H., Zahnle, K.J., Kasting, J.F., and Morowitz, H.J. (1989) Annihilation of ecosystems by large asteroid impacts on the early Earth. *Nature* 342, 139–142.

Smit, J. (1999) The global stratigraphy of the Cretaceous-Tertiary boundary impact ejects. *Annu. Rev. Earth Planet. Sci.* 27, 75–113.

Smit, J., Roep, Th.B., Alvarez, A., Montarari, A., Claeys, P., Grajales-Nishimura, J.M., and Bermudez, J. (1996) Coarse-grained, clastic sandstone complex at the K/T boundary around the Gulf of Mexico: deposition by tsunami waves induced by the Chicxulub impact. In *Special Paper 307: The Cretaceous-Tertiary Event and Other Catastrophes in Earth History*, edited by G. Ryder, D. Fastovsky, and S. Gartner, Geological Society of America, Boulder, CO, pp. 151–182.

Smith, H.S. and Erlank, A.J. (1982) Geochemistry and petrogenesis of komatiites from the Barberton Greenstone Belt, S.A. In *Komatiites*, edited by N.T. Arndt, M. Bickle, and E.G. Nisbet, Allen and Unwin, London, pp. 347–394.

Stanistreet, I.G., de Wit, M.J., and Fripp, R.E.P. (1981) Do graded units of accretionary spheroids in the Barberton greenstone belt indicate Archaean deep water environment? *Nature* 293, 280–284.

Stevenson, D.J. (1985) Implications of very large impacts for Earth accretion and lunar formation. In *16th Lunar and Planetary Science Conference, Abstracts, Pt. 2*, Lunar and Planetary Institute, Houston, pp. 819–820.

Stevenson, D.J. (1987) Origin of the Moon—the collision hypothesis. *Annu. Rev. Earth Planet. Sci*. 15, 271–315.

Tera, F., Papanastassiou, D.A., and Wasserburg, G.J. (1974) Isotopic evidence for a terminal lunar cataclysm. *Earth Planet. Sci. Lett*. 22, 1–21.

Tredoux, M., de Wit, M.J., Hart, R.J., Armstrong, R.A., Lindsay, N.M., and Sellchop, J.P.F. (1989) Platinum group elements in a 3.5 Ga nickel-iron occurrence: possible evidence of a deep mantle origin. *J. Geophys. Res.* 94, 795–813.

Xie, X., Byerly, G.R., and Ferrell, R.E. (1997) IIb trioctahedral chlorite from the Barberton Greenstone Belt: crystal structure and rock composition constraints with implications to geothermometry. *Contrib. Mineral. Petrol.* 126, 275–291.

Zahnle, K.J. and Sleep, N.H. (1997) Impacts and the early evolution of life. In *Comets and the Origin and Evolution of Life*, edited by P.J. Thomas, C.F. Chyba, and C.P. McKay, Springer, New York, pp. 175–208.

Address reprint requests to:
Dr. Donald R. Lowe
Department of Geological
and Environmental Sciences
Stanford University
Stanford, CA 94305–2115

E-mail: lowe@pangea.Stanford.edu

LOWE

AU1
update yet?

AU2
update yet?

QU1
3 head OK as set. We follow #3 head specs instead of manuscript. Which is correct style, initial cap/lc or cap/lc. Please note our spec for a #4 head is initial cap/lc.